(3)

[redacted]

Eugene E. Covert and Peter F. Lurie

[redacted]

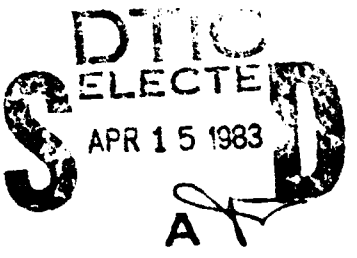

DEPARTMENT OF
AERONAUTICS AND ASTRONAUTICS
MASSACHUSETTS INSTITUTE OF TECHNOLOGY
CAMBRIDGE, MASSACHUSETTS 02139

UNSTEADY PRESSURE AND BOUNDARY LAYERS ON AN 0012 AIRFOIL CAUSED BY AERODYNAMIC INTERFERENCE

by

Eugene E. Covert and Peter F. Lorber

August 1982

This research was supported by the Air Force Office of Scientific Research under Contract No. AFOSR-80-0282, Capt. Michael S. Francis, Program Manager.

UNCLASSIFIED

SECURITY CLASSIFICATION OF THIS PAGE *(When Data Entered)*

REPORT DOCUMENTATION PAGE	READ INSTRUCTIONS BEFORE COMPLETING FORM
1. REPORT NUMBER: AFOSR-TR- 83-0200 AD-A126 999	2. GOVT ACCESSION NO. / 3. RECIPIENT'S CATALOG NUMBER
4. TITLE *(and Subtitle)*: UNSTEADY PRESSURE AND BOUNDARY LAYERS ON AN 0012 AIRFOIL CAUSED BY AERODYNAMIC INTERFERENCE	5. TYPE OF REPORT & PERIOD COVERED: ANNUAL, 1 Sep 81 - 31 Aug 82
	6. PERFORMING ORG. REPORT NUMBER
7. AUTHOR(s): EUGENE E COVERT, PETER F LORBER	8. CONTRACT OR GRANT NUMBER(s): AFOSR-80-0282
9. PERFORMING ORGANIZATION NAME AND ADDRESS: MASSACHUSETTS INSTITUTE OF TECHNOLOGY, DEPARTMENT OF AERONAUTICS & ASTRONAUTICS, CAMBRIDGE, MA 02139	10. PROGRAM ELEMENT, PROJECT, TASK AREA & WORK UNIT NUMBERS: 61102F, 2307/A2
11. CONTROLLING OFFICE NAME AND ADDRESS: AIR FORCE OFFICE OF SCIENTIFIC RESEARCH/NA, BOLLING AFB, DC 20332	12. REPORT DATE: Aug 82
	13. NUMBER OF PAGES: 47
14. MONITORING AGENCY NAME & ADDRESS *(if different from Controlling Office)*	15. SECURITY CLASS. *(of this report)*: Unclassified
	15a. DECLASSIFICATION DOWNGRADING SCHEDULE

16. DISTRIBUTION STATEMENT *(of this Report)*

Approved for Pubic Release; Distribution Unlimited.

17. DISTRIBUTION STATEMENT *(of the abstract entered in Block 20, if different from Report)*

18. SUPPLEMENTARY NOTES

19. KEY WORDS *(Continue on reverse side if necessary and identify by block number)*

GROUND TESTING	UNSTEADY BOUNDARY LAYER
WIND TUNNEL	SEPARATED FLOW
UNSTEADY FLOW	DYNAMIC STALL

20. ABSTRACT *(Continue on reverse side if necessary and identify by block number)*

Aerodynamic characteristics have been measured for a NACA 0012 airfoil in a non-uniform unsteady flow field. Test parameters studied included reduced frequencies based on semichord of 0 to 6.4 Reynolds number of 700,000 to 1,450,000, and airfoil angles of attack of 0 to 15°. Quantities measured were upwash velocity fields, turbulent boundary layer velocities and Reynolds stresses, and attached and separated flow pressure distributions. The influence of frequency, pressure gradient, unsteady amplitude and measurement location are discussed. Results are compared with previous results and physical

DD FORM 1 JAN 73 1473 EDITION OF 1 NOV 65 IS OBSOLETE

UNCLASSIFIED

SECURITY CLASSIFICATION OF THIS PAGE *(When Data Entered)*

models for steady and unsteady flows. Superposition of unsteady and mean quantities appears to be valid for low pressure gradient attached flow, but becomes increasingly inadequate as separation is approached. Propagation of unsteady pressures in separated flow resembles a superposition of a disturbance convected downstream from the leading edge onto the standing wave pattern found in attached flow, but includes numerous additional complexes.

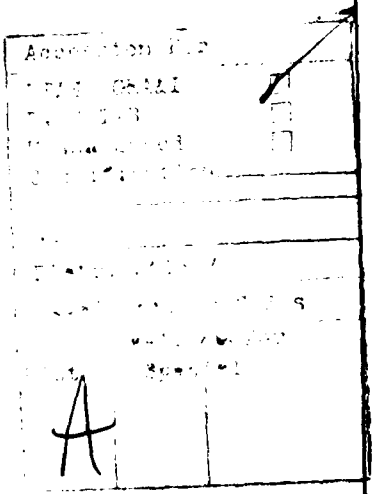

UNSTEADY PRESSURE AND BOUNDARY LAYERS ON AN 0012 AIRFOIL CAUSED BY AERODYNAMIC INTERFERENCE

Eugene E. Covert

Peter F. Lorber

Massachusetts Institute of Technology
Department of Aeronautics & Astronautics
Cambridge, MA 02139

Annual Report

September 1, 1981
August 31, 1982

Contract # AFOSR-80-0282

TABLE OF CONTENTS

TECHNICAL SUMMARY

Continued progress has been made in the past year in understanding the unsteady flow about an airfoil. Experimental data have been obtained describing the unsteady pressures on the airfoil surface for conditions ranging from attached flow at zero angle of attack to separated flow at 15° angle of attack. To complement these data, the unsteady flow field that produces these pressures has been measured for the same range of test conditions, but with no airfoil present in the wind tunnel. Boundary layer measurements, including ensemble averages of 2 velocity components and 3 Reynolds stresses have been made over a range of attached flow conditions. Finally, wake surveys have been made for 50 combinations of the parameters Reynolds number, perturbation frequency, angle of attack, and downstream position.

Interpretation of this considerable quantity of data is continuing, with some progress having been made in identifying the key features of the flow field, and in determining the relative significance of the numerous parameters involved. Work has continued on the development of numerical techniques to predict the unsteady boundary layers and wakes based on the airfoil pressure distributions and to predict the pressures based upon the unsteady velocity field.

The present report is divided into several largely independent sections. First, a brief summary of the experimental apparatus and technique is given. Second, some of the results of the measurements of the unsteady velocity field are presented. Third, the results of measurements made to date on the pressure field of the stalled airfoil are given. Fourth, earlier work on

the airfoil surface pressures and their relation to the velocity field is discussed by a copy of a recently published paper (Appendix A). Finally, a copy of a paper giving the current results on the unsteady boundary layer is included (Appendix B). Since the measurements of the wake were completed only at the end of the year, a report on this data will be given at a later date.

EXPERIMENTAL APPARATUS AND PROCEDURE

Since this experiment has been described at some length previously (1,2,3), only a brief summary is included here. As shown in Figure 1, the experimental apparatus consists of 2-dimensional NACA 0012 airfoil which may be mounted at fixed angle of attack between sidewalls in a low speed wind tunnel. Unsteady flow is generated by rotating an elliptic cylinder located behind and beneath the airfoil trailing edge. Test Reynolds numbers ranged from 7×10^5 to 1.4×10^6 based on airfoil chord, while reduced frequencies, $k = \omega c/2U_\infty$ varied between 0.5 and 6.4.

Airfoil pressures were measured at 35 locations on the upper and lower surface, while either single or cross hot wires measured local velocities. A new computer-controlled stepping motor probe drive system was introduced this year for use in taking wake profiles. This system both speeds data acquisition and increases the maximum traverse from 10cm to 21cm.

Data for both pressures and velocities are required digitally as shown in Figure 2 and described in Reference 3. Data storage, processing and display techniques are also discussed in that reference.

TESTS OF THE INDUCED VELOCITY FIELD

To define the unsteady flow field generated by the rotating elliptic cylinder, the airfoil is removed from the wind tunnel and hotwire anemometer measurements are made of the vertical and horizontal velocity components along the position of the airfoil chord. As reported in References 1, 2 and 4 such data were taken along a line corresponding to an airfoil at 0 angle of attack, at position A, as shown in Figure 3. Thin airfoil theory was then used on the data to predict the unsteady difference pressures on an airfoil at that location. The prediction was then compared to the measured pressure distribution on the NACA 0012 airfoil (1, 2, 3, 4.)

Following these initial measurements, airfoil pressure data have also been taken at 3 additional positions (Figure 3). In position B the airfoil is rotated 10° nose up about the trailing edge from position A. In position C the distance between the elliptic cylinder and the airfoil trailing edge is reduced while maintaining 10° angle of attack. In position D the airfoil is rotated about the trailing edge to 15° angle of attack, while maintaining airfoil-ellipse distance as in position C.

Since the induced velocity field at these additional positions differs from that at position A, an additional series of elliptic-cylinder alone velocity measurements were required to determine this difference. These tests were performed in November 1981, using the digital data acquisition and processing system that had been developed since the original analog measurements were made (Figure 2, Reference 3). The u and v velocity components were measured at 21 locations which covered the 4 chord positions. Data were taken at 2 Reynolds numbers (7 and 10 x 10^5 based on airfoil chord) and at steady and 5 unsteady elliptic cylinder frequencies ($0.5 \leq k \leq 6.4$).

Allowing for repeated runs, 268 test points in (position, Re, k) space were taken.

The qualitative features of the ensemble average induced upwash (v) velocity field may be seen in Figures 4 and 5. These figures are 3-dimensional plots of the upwash as a function of time and distance along the position of the airfoil chord. Time has been nondimensionalized so that 720° corresponds to 1 elliptic cylinder revolution. Distance from the leading edge position is nondimensionalized by the airfoil chord, and velocity by the freestream velocity. Both figures are at $Re = 7 \times 10^5$ and chord position A. Figure 4 is for $k = 1.0$, and shows the typical character of the upwash: both mean and unsteady velocities increase sharply as the trailing edge position and the elliptic cylinder are approached; the waveform is roughly sinusoidal in time; and the shift in phase with distance along the chord is small. Figure 5, for $k = 3.9$, is qualitatively similar, but is characterized by higher mean upwash velocities and lower unsteady amplitudes.

Mean upwash distributions for the two extreme steady elliptic cylinder orientations at position C are shown in Figure 6. The upwash for the horizontal ellipse shown is based on a potential flow calculation. This upwash is used as the reference upwash, and is needed for the cross hot-wire anemometer calibration (1). The upwash for the vertical ellipse shown is a sum of this reference upwash and the measured difference in upwash between the vertical and horizontal cases. The dashed line in Figure 6 is a potential flow calculation for the vertical ellipse. Naturally, it does not account for the large regions of separated flow which exist behind the vertical ellipse. The procedure of adding a calculated reference upwash to a measured difference in upwash was followed for all steady and unsteady cases and is explained in Ref. 1. Note that this procedure includes tunnel non-uniformities in the reference flow.

To get quantitative information on the upwash distributions, the ensemble average waveform such as in Figure 4 and 5 is Fourier analyzed, and the amplitude and phase lag of the harmonics of the ellipse rotation rate are found. The fundamental harmonic is defined to be twice the ellipse rotation rate. Figure 7 presents amplitude data for $Re = 7 \times 10^5$, $k = 1$, position C. Harmonic 0 is the mean, 0.5 the subharmonic, and 1 the fundamental. The distributions of the mean and of the fundamental confirm the qualitative features discussed above, while those for the sub and higher harmonics confirm the essentially sinusoidal nature of the flow. Note that while the original prediction of unsteady airfoil pressure (Ref. 1) considered only the first harmonic, the effect of the other harmonics may be added if desired.

Figure 8 presents the same quantities for $k = 3.9$. The major differences from the $k = 1$ results in Figure 7 are the reduced unsteady amplitudes, the somewhat larger mean amplitudes, and the smaller mean amplitude for $x/c > 1$.

Phase lag distributions for position C, $Re = 7 \times 10^5$ and $0.5 < k < 6.4$ are shown in Figure 9 as a function of x/c. A phase lag of 0 means that the minimum upwash occurs when the elliptic cylinder is horizontal. All of the frequencies are characterized by nearly constant phase lag for $x/c < 0.8$, with an increase in phase lag for $x/c > 0.8$. For $k \leq 1$, this increase is approximately 20°, where, as before, 720° corresponds to one elliptic cylinder rotation. At $k = 2$ the increase is of the same magnitude, but the phase lag is about 40° larger at all points along the chord than at $k < 2$. For $k > 2$ the phase lag at all points drops again, with values

for k = 6.4 being approximately 60° less than the values for k = 1 at the same position. The increase in phase between x/c = 0.8 and x/c = 1.1 is larger when k > 2, reaching 45° for k = 6.4.

For the present purposes, the details of the flow field are less important than the fact that the phase is relatively constant along a chord line, for a given frequency, Reynolds number and trailing edge position. In contrast, if the flow field was due to a sinusoidal gust convected at a uniform velocity U_g, the phase distribution would be described by:

$$\frac{d\phi}{dx} = \frac{\omega}{U_g} , \quad \text{or} \quad \frac{d\phi}{d(x/c)} = \frac{2k}{(U_g/U_\infty)} ,$$

which yields a phase difference between the leading and trailing edges of $\Delta\phi = 2kU_\infty/U_g$ radians. For $U_g = U_\infty$ and k = .5, $\Delta\phi$ = 57.3°, while for k = 6.4, $\Delta\phi$ = 734°, almost fifteen times larger than the measured values. Therefore the assumption of a fixed or at best a slowly convected disturbance seems reasonable.

Note that a correction to the unsteady thin airfoil theory to account for the small convective component of the upwash may be made (4). This correction makes an insignificant change in the resulting pressure distributions under the conditions studied here.

To obtain a more global picture of the dependence of the induced upwash on the parameters Re, α, k, and position, the upwash at the trailing edge location was selected as a reference. This choice reflects both the importance of the trailing edge in determining airfoil flows, and the fact that the maximum upwash occurs there. Figure 10 shows the mean flow angle (arctangent (v/u)) with respect to the airfoil chord line, plotted against reduced frequency for the 4 positions and the 2 Reynolds numbers studied.

In general the mean flow angle at the trailing edge shows little dependence on Re or k, being influenced chiefly by the airfoil angle of attack and the distance to the elliptic cylinder. Thus results for position B are 10° higher than for A due to angle of attack, and results for C are 5-7° higher than for D due to reduced trailing edge-elliptic cylinder distance.

Figure 11 shows the amplitude of the fundamental harmonic of the flow angle for the same conditions. The Reynolds number dependence is larger than that seen in the mean angle, but is still small compared to the frequency dependence. The Reynolds number effect is larger nearer to the elliptic cylinder, where the details of the flow over it are more important than they are further away. Due to the increased acceleration needed to move the fluid at higher frequencies, the amplitude is reduced. The dependence on position is strong, with amplitudes for positions C and D 50% larger than for A and B at $k < 1$, and up to 200% larger at $k = 6.4$. The phase lag at the trailing edge, as shown in Figure 12, has a similar weak dependence on Reynolds number, and a strong dependence on frequency and distance. Phase lags appear to approach 0 as k approaches 0, in agreement with steady incompressible flow, where the propagation speed is infinite.

To conclude, these more complete and detailed studies of the induced velocity fields largely confirm trends observed earlier, extending them to the wider range of parameters (k, α, Re, position) currently studied. The field depends smoothly on space and time, with maximum amplitudes concentrated near the position of the airfoil trailing edge, and unsteady components dominated by the fundamental harmonic. Reynolds number dependence is small away from the immediate vicinity of the elliptic cylinder.

The frequency dependence of the unsteady component of the flow is always significant. No qualitative changes were seen in the field due to changes in airfoil position relative to the ellipse. Unsteady amplitudes were, as desired, significantly increased by moving the trailing edge closer to the elliptic cylinder. Phase lag distribution along the chord was studied in more detail than previously possible. The chordwise variation of phase was found to be small and is much smaller than that expected if a disturbance is convected at the free stream velocity.

PRESSURE DISTRIBUTION ON THE STALLED AIRFOIL

In uniform steady flow, the NACA 0012 airfoil has been found to stall at an angle of attack of approximately 16°, at a lift coefficient of 1.5 (7). These values are for $Re = 3 \times 10^6$, the lowest value given. In the present study the airfoil is in the non-uniform unsteady flow generated by the rotating elliptic cylinder, so that the conditions causing stall are different, as will be discussed below.

Stall was observed for position C at $\alpha = 10°$ only for $k = 6.4$ and $Re = 7 \times 10^5$, and for all frequencies and Reynolds numbers studied at position D at $\alpha = 15°$. The stall was characterized by a separation of the boundary layer on the upper surface starting near the leading edge and extending over the entire surface. No dynamic stall, or oscillatory separation and reattachment was seen. The unsteady pressures generated by the rotating elliptic cylinder propagated through the separated flow region, but the essential character of the flow remained constant.

The first case to be discussed is the separated flow that may occur at $\alpha = 10°$, $k = 6.4$ and $Re = 7 \times 10^5$. Under these conditions both attached and separated flow states are possible. The mean pressure distributions for these two states are shown in Figure 13. The attached flow is characterized by a suction peak on the upper surface at $x/c = .025$ of $c_p = -6.2$, while the separated flow has a nearly uniform mean upper surface pressure of $-1 < c_p < -0.5$. The lower surface pressures are almost the same for the two states, largely unaffected by the stall. The flow may remain attached for times up to an hour, or until a disturbance large enough to trip the flow passes the airfoil. Once

separated the flow has never been observed to spontaneously reattach. If the reduced frequency is reduced to approximately k = 1, the flow is reattached and the frequency may again be increased to k = 6.4. This hysteresis seems typical of stalled flows. (Ref. 8).

Ensemble averaged unsteady pressure distributions may be compared to the 2 cases. Approximately 400 cycles of averaging are required to define the flow in the separated case, while only 200 are sufficient for the attached flow. Figure 14 shows upper and lower surface fundamental harmonic amplitude distributions. The lower surface distribution is seen to be relatively unaffected by the separation, with pressure amplitudes uniformly increased by about 15% by separation. The upper surface distribution is quite different, as separation appears to superimpose a damped sinusoidal oscillation on the smoothly varying attached distribution. The phase lag distributions in Figure 15 show similar behavior. The lower surface is virtually unaffected, while an oscillation in phase is superimposed on the upper surface for $x/c < 0.8$.

By inserting phase jumps of 2π at $x/c = 0.05$ and 0.3 a region of monotonic increase in phase lag for $.025 < x/c < 0.4$ is obtained, such as that shown later in Figure 24. A linear fit in this region gives results similar to those of a disturbance propagating downstream at a phase velocity of $0.5\ U_\infty$. That the situation is more complex than a simple propagating wave is apparent from the amplitude distribution, but the picture of pressure disturbances from the lower surface moving around the leading edge and propagating downstream after the stagnation point may be useful. A similar result was obtained by a study of the fluctuating pressures on a steady airfoil (8).

At airfoil position D, where the angle of attack is 15°, all 5 unsteady frequencies ($0.5 \leq k \leq 6.4$) studied, plus the case of a steady vertical

elliptic cylinder at both test Reynolds numbers of 7 and 10 x 10^5 were stalled. Only the case of a steady horizontal elliptic cylinder had attached flow. Figure 16 shows the mean pressure distributions at Re = 10^6 for all studied frequencies. As in the previous stalled case, the lower surface is relatively unaffected, while the upper surface pressure distribution is flat at $-1 < c_p < -0.5$. Frequency dependence is exhibited primarily on the upper surface: leading edge pressures are higher for $k < 2$, a low pressure bump develops at $k = 2$, and more variation with x is seen near the leading edge for $k > 2$.

A more quantitative picture is obtained by examining the mean and unsteady lift coefficients. Figure 17 presents the mean lift coefficient as a function of frequency for both the stalled $\alpha = 15°$ data and the attached $\alpha = 10°$ data for the same trailing edge position relative to the ellipse. The attached flow mean lift coefficient increases with k, primarily due to the increased circulation produced by spinning the elliptic cylinder faster, reading a maximum of $C_L = 1.46$ for $k > 5$. This value is more or less equal to the maximum C_L for the NACA 0012 airfoil in steady uniform flow (7). However, if the unsteady lift coefficient is added to the mean, the instantaneous values of C_L become as large as 1.6, greater than the steady maximum. These results may be compared with those obtained by rotating the NACA 0012 in uniform flow, such as by McCroskey, Carr and McAlister (9). In these tests the Reynolds number is somewhat larger, Re = 2.5 x 10^6, the frequency lower, $k \leq 0.25$, and the amplitude much greater, $5° \leq \alpha \leq 25°$. Instantaneous maximum lift coefficients were found to be much greater than the maximum in steady flow, but when averaged over the airfoil rotation period, the mean lift coefficient was much closer to the steady flow value.

Mean C_L increases with Reynolds number, also in agreement with the high lift results in Ref. 7. The stalled flow lift coefficients are always lower, with the difference between being less than 10% for $k \leq 2$, and becoming 30% lower for the

deeper stall case at $k > 5$. As in the pressure distributions in Figure 16, the behavior changes significantly at $k = 2$. The reasons for this change are not known.

The unsteady lift coefficient is relatively unaffected by the stall of the mean flow. Figure 18 shows the amplitude of the fundamental harmonic for the cases discussed above. The attached flow data re in qualitative agreement with earlier results for positions A and B (Ref. 3), and after the mean flow separates the first harmonic still follows the same trends: C_L drops for $k > 1$, has a minimum at $k \sim 2$ and then increases for $k > 2$. Phase lags for C_L, as shown in Figure 19, are also qualitatively similar for the attached and separated mean flows, with the primary difference being a 45° higher phase lag for $k \leq 1$.

The ensemble averaged pressure distribution is shown in the next series of figures, which are 3-dimensional plots of the pressure coefficient as a function of non-dimensional time and distance from the airfoil leading edge. Each curve is an average of 400 cycles. Figure 20 shows the pressures on the lower surface for $k = 1$, $\alpha = 15°$, and $Re = 10^6$. As would be expected from the curves discussed earlier, the pressure distribution is similar to lower surface distributions for unstalled cases, and is characterized by large unsteady amplitudes and small phase differences along the chord (Ref. 3). Figure 21 shows the upper surface for the same conditions. Note that the x/c axis has been reversed for clarity in Figure 21. In the trailing edge region the pressure is similar to that for unstalled flows, with large amplitudes and small phase shifts. From the leading edge to midchord the amplitude varies relatively rapidly, and the phase lag increases monotonically. This is consistent with the results shown in Figure 14 and 15 at $\alpha = 10°$. The difference pressure coefficient, $C_{p,lower} - C_{p,upper}$, is shown in Figure 22. It includes both the nearly constant phase lower surface wave form and the rapidly varying upper surface disturbance,

resulting in a pattern quite different from that of an unstalled flow. The interface between these two regions near midchord appears for this reason to have a frequency doubling.

Data for higher reduced frequencies are similar, but not as clearly defined, due primarily to the more rapid phase variation, a result of a decrease wavelength to chord ratio. No significant Reynolds number effect was seen on the ensemble averaged pressure coefficients.

The exception to this behavior is the region near the trailing edge of the upper surface at $k = 0.5$, as seen in Figure 23 for $Re = 7 \times 10^5$. A frequency doubling develops for $x/c > 0.9$, due perhaps to a coupling with the vortex shedding from the slowly rotating elliptic cylinder. The same effect is present at $Re = 10^6$.

As discussed above for the $\alpha = 10°$ data, one interpretation of the pressure distribution on the upper surface is in terms of the propagation of a travelling disturbance downstream from the leading edge. The ensemble average pressure may be represented as

$$\langle p \rangle (x,t) = \bar{p}(x) + \tilde{p}_1(x)\cos(\omega t - \phi(x)) + \tilde{p}_2(x,t),$$

where $\tilde{p}_2(x,t)$ contains harmonics other than the fundamental. For a disturbance propagated at a constant speed U_{wave}, the phase lag $\phi(x)$ is $\omega x/U_{wave}$. Therefore the wave velocity is defined as $U_{wave} = \omega/(d\phi/dx)$, or in non-dimensional terms $U_{wave}/U_\infty = 2k/(cd\phi/dx)$. If the mean flow velocity $U_e(x)$ is introduced, its ratio with this wave velocity becomes

$$U_{wave}/U_e = \frac{2k}{c\frac{d\phi}{dx}\sqrt{1-\bar{c}_p}} \quad .$$

Figure 24 shows the phase lag, $\phi(x)$, for two representative cases at $\alpha = 15°$, $Re = 10^6$. For $k = 1$ the phase increases smoothly and monotonically, but not linearly as in the simple model above. For $k = 4$ the data is similar, but more complex, as seen in the jump in phase near $x/c = .5$ and in the maximum at $x/c = .75$, followed by a slight drop in phase lag as the trailing edge is approached.

Figure 25 shows the linear propagation velocity U_{wave}/U_e for these same two cases. For $k = 1$ the variations are smooth, U_{wave} is always positive and normally in the range $0.2 < U_{wave}/U_e < 1.2$, consistent with a disturbance propagating downstream. The situation is much more complex at $k = 4$, where the wave speed varies much more rapidly, reaching extremes of $+6\tilde{U}_e$ and $-3\tilde{U}_e$. The negative wave velocities for $x/c \geq 0.85$ seem to indicate an upstream propagation in this region. The interaction between this disturbance and that propagating downstream from the leading edge may account for the unusual behavior for $0.6 < x/c < 0.8$. Another possible cause is interaction with the two-dimensional channel surrounding the airfoil.

The propagation of disturbances in separated flow is obviously a very complex process, and not a simple travelling wave or sum of travelling waves, as with a convected gust. The process is highly frequency dependent, with the complexity increasing rapidly for $k > 1$.

In conclusion, some of the main characteristics of the separated flow about an airfoil in our particular unsteady, non-uniform flow field have been discussed. Many of these characteristics, in particular those dealing with conditions for separation, the mean pressure distribution, and the behavior of the lift coefficient appear to agree with results of earlier attached flow data and other results for stalled flow. The unsteady pressure distribution at the fundamental harmonic seems relatively unaffected by the outer mean flow separation. However, other characteristics, primarily

those concerned with the propagation of unsteady pressures in the separated flow are more complex and resist straightforward explanations. More effort, both conceptual, in interpreting the existing data, and experimental, primarily in adding velocity measurements to go with the pressure data, is necessary in order to reach an improved understanding of the process(es).

REFERENCES

1. Lorber, P.F. and Covert, E.E., "Preliminary Results of a Study of Unsteady Airfoil Surface Pressures and Turbulent Boundary Layers," M.I.T. Aerophysics Lab TR 210, December 1980.

2. Lorber, P.F., "Unsteady Airfoil Pressures Induced by Perturbation of the Trailing Edge Flow," SM Thesis Aeronautics and Astronautics Department, M.I.T., February 1981.

3. Lorber, P.F., and Covert, E.E., "Additional Results of a Study of Unsteady Airfoil Surface Pressures and Turbulent Boundary Layers," M.I.T. Aerophysics Lab TR 212, also AFOSR-TR-81-0848TR, November 1981.

4. Lorber, P.F., and Covert, E.E., "Unsteady Airfoil Pressures Produced by Periodic Aerodynamic Interference," AIAA Journal, 20, September 1982, pp.1153-1159.

5. Covert, E.E., and Lorber, P.F., "Unsteady Turbulent Boundary Layers in Adverse Pressure Gradients," AIAA paper 82-0966, submitted to AIAA Journal in July 1982.

6. Covert, E.E., Lorber, P.F., and Vaczy, C.M., "Measurements of the Near Wake of an Airfoil in Unsteady Flow," to be presented as AIAA paper 83-0127 at the AIAA 21st Aerospace Sciences Meeting, Reno, Nevada, January, 1983.

7. Abbot, I.H. and von Doenhoff, A.E., "Theory of Wing Sections," Dover Publications, Inc., New York, 1959, p.321.

8. St. Hilaire, A.O., Carta, F.O., Fink, M.R., and Jepson, W.D., "The Influence of Sweep on the Aerodynamic Loading of an Oscillating NACA 0012 Airfoil," NASA CR-3092, May 1979.

9. McCroskey, W.J., Carr, L.W. and McAlister, K.W., "Dynamic Stall Experiments on Oscillating Airfoils," AIAA Journal, 14, January 1976, pp.57-63.

LIST OF SYMBOLS

c	airfoil chord
c_L	section lift coefficient, $L/(1/2\rho U_\infty^2 C)$
c_p	pressure coefficient, $(P-P_{static})/(1/2\rho U_\infty^2)$
k	reduced frequency, $\omega c/2U_\infty$
L	section lift
p	pressure
p_{static}	freestream static pressure
$\bar{p}$	time averaged pressure
$<p>$	ensemble averaged pressure
$\tilde{p}_1$	fundamental harmonic of $<p>$
$\tilde{p}_2$	other harmonics of $<p>$
Re	Reynolds number, $U_\infty c/\nu$
t	time
u	tangential velocity
U_e	external velocity, at boundary layer edge
U_g, U_{wave}	gust velocity, propagation velocity of a disturbance
v	normal velocity
x	tangential coordinate
y	normal coordinate
α	angle of attack, with respect to freestream velocity
ν	kinematic viscosity
ρ	density
ϕ	phase angle
ω	radian frequency

Status of Research

1. Earlier conclusions as to the nature and superposability of the unsteady pressure field on the mean pressure field and the applicability of unsteady thin airfoil theory have been confirmed and extended from the zero angle of attack to higher angles of attack.

2. A series of tests on the pressure distribution in stalled flow have resulted in a collection of data revealing many characteristics of the flow. Further thought, interpretation and investigation is required, in particular with regard to the origin and nature of pressure disturbances in this flow.

3. Boundary layer measurements have been taken over a wide range of pressure gradients and frequencies, allowing determination of some of the key features of the unsteady boundary layer and of the influence of the important parameters. More work is required in order to measure profiles at more stations at each configuration, to get a better picture of the development of the boundary layer. Continued development of numerical techniques to predict the boundary layer with reasonable accuracy is also required.

4. Wake profiles have been taken over a similarly wide segment of parameter space, and will provide a data base for increasing understanding of this little investigated portion of the unsteady flow.

5. Development of a shear gauge to measure unsteady skin friction has been slowed by the persistent drift in the electronic circuits. Presently this effort is on hold due to lack of a suitable research assistant. We are considering the use of other techniques that have been developed recently to determine this important parameter.

Cumulative Publications

1. Lorber, P.F. and Covert, E.E., "Unsteady Airfoil Pressures Produced by Periodic Aerodynamic Interference," AIAA Journal, 20, September 1982, pp.1153-1159.

2. Covert, E.E., and Lorber, P.F., "Unsteady Turbulent Boundary Layers in Adverse Pressure Gradients," AIAA paper 82-0966, submitted to AIAA Journal in July 1982.

3. Covert, E.E., Lorber, P.F., and Vaczy, C.M., "Measurements of the Near Wake of an Airfoil in Unsteady Flow," accepted for presentation as AIAA paper 83-0127 at the AIAA 21st Aerospace Sciences Meeting, Reno, Nevada, January 1983.

Professional Personnel

The following people have contributed to this project in the past year:

1.	Professor E.E. Covert	Principal Investigator
2.	P.F. Lorber	Research Assistant
3.	R. Lee (up to June 1982)	Research Assistant
4.	C.M. Vaczy (after June 1982)	Research Assistant

Interactions

The paper "Unsteady Turbulent Boundary Layers in Adverse Pressure Gradients" was presented at the AIAA/ASME 3rd Joint Thermophysics, Fluids, Plasma and Heat Transfer Conference, held June 7-11, 1982 in St. Louis, MO.

We have discussed the unsteady data with Professor Dennis Whitehead of the Whittle Laboratory with a view of application of his Finite Element Technique to assist interpretation of data.

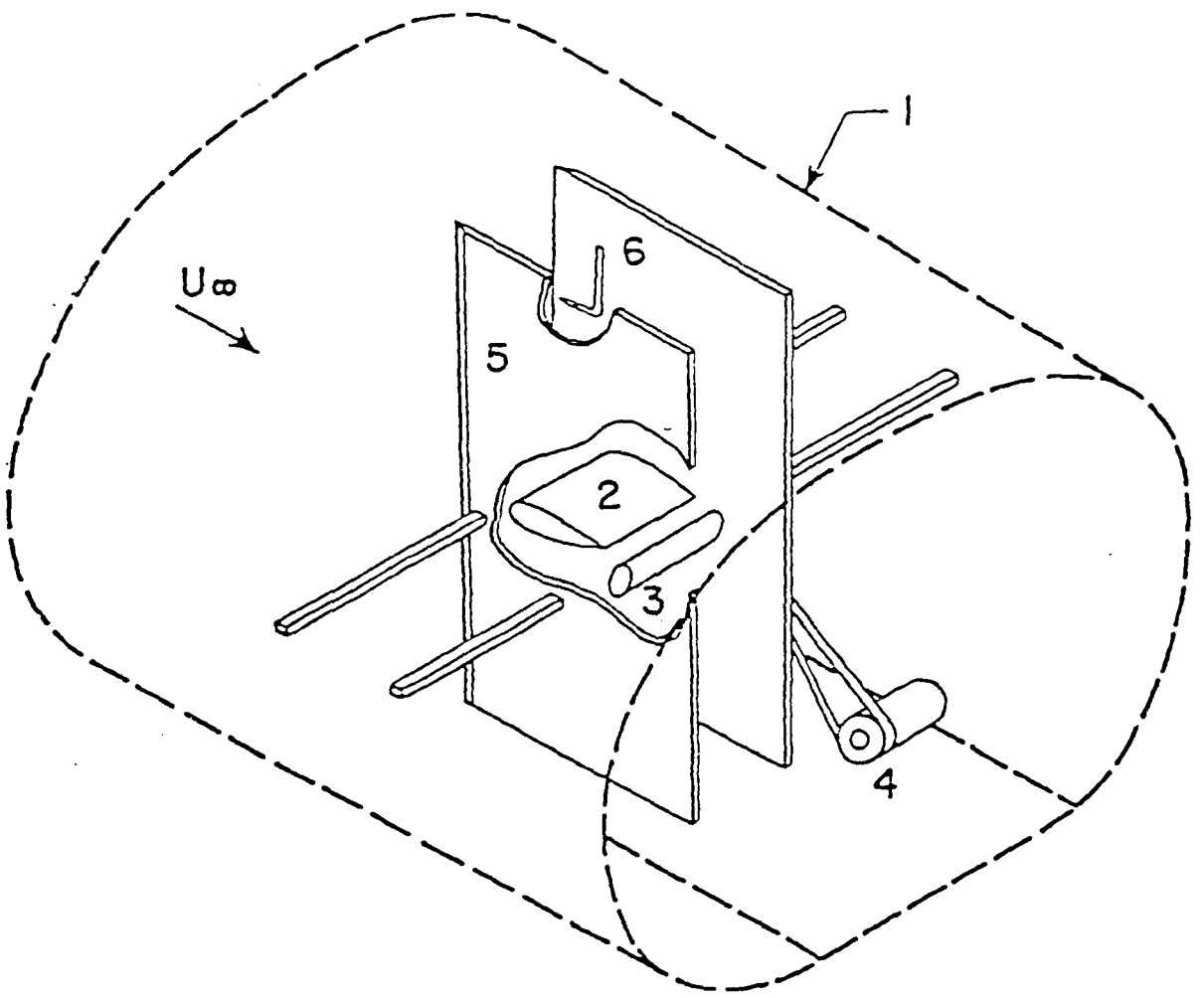

1) Test Section

2) NACA 0012 Airfoil

3) Rotating Elliptic Cylinder

4) Drive Motor (0-3300 rpm)

5) 2-D Sidewalls

6) Pitot-Static Probe

FIGURE 1

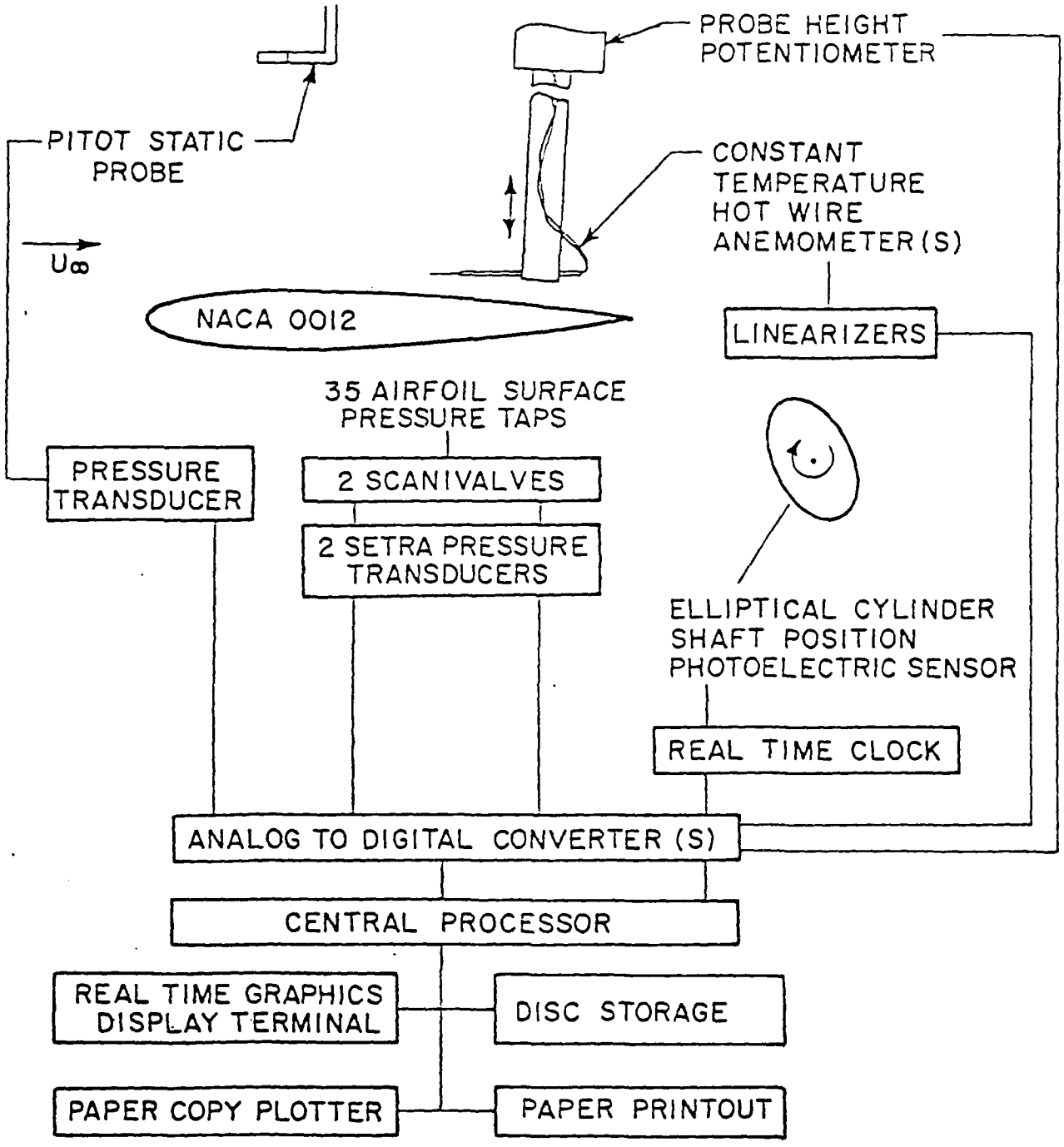
PROBE HEIGHT POTENTIOMETER
PITOT STATIC PROBE
CONSTANT TEMPERATURE HOT WIRE ANEMOMETER(S)
U_∞
NACA 0012
LINEARIZERS
35 AIRFOIL SURFACE PRESSURE TAPS
PRESSURE TRANSDUCER
2 SCANIVALVES
2 SETRA PRESSURE TRANSDUCERS
ELLIPTICAL CYLINDER SHAFT POSITION PHOTOELECTRIC SENSOR
REAL TIME CLOCK
ANALOG TO DIGITAL CONVERTER (S)
CENTRAL PROCESSOR
REAL TIME GRAPHICS DISPLAY TERMINAL
DISC STORAGE
PAPER COPY PLOTTER
PAPER PRINTOUT

FIGURE 2

AIRFOIL POSITIONS

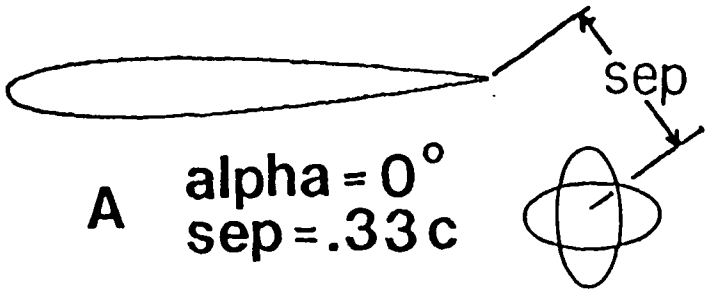

A alpha = 0°
sep = .33c

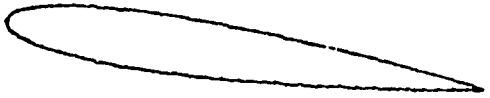

B alpha = 10°
sep = .33c

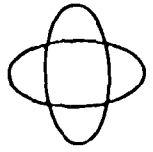

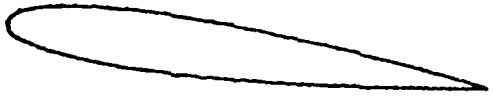

C alpha = 10°
sep = .22c

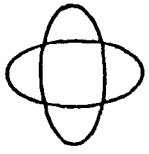

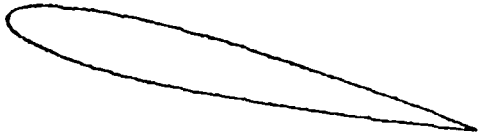

D alpha = 15°
sep = .22c

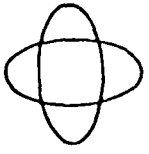

FIGURE 3

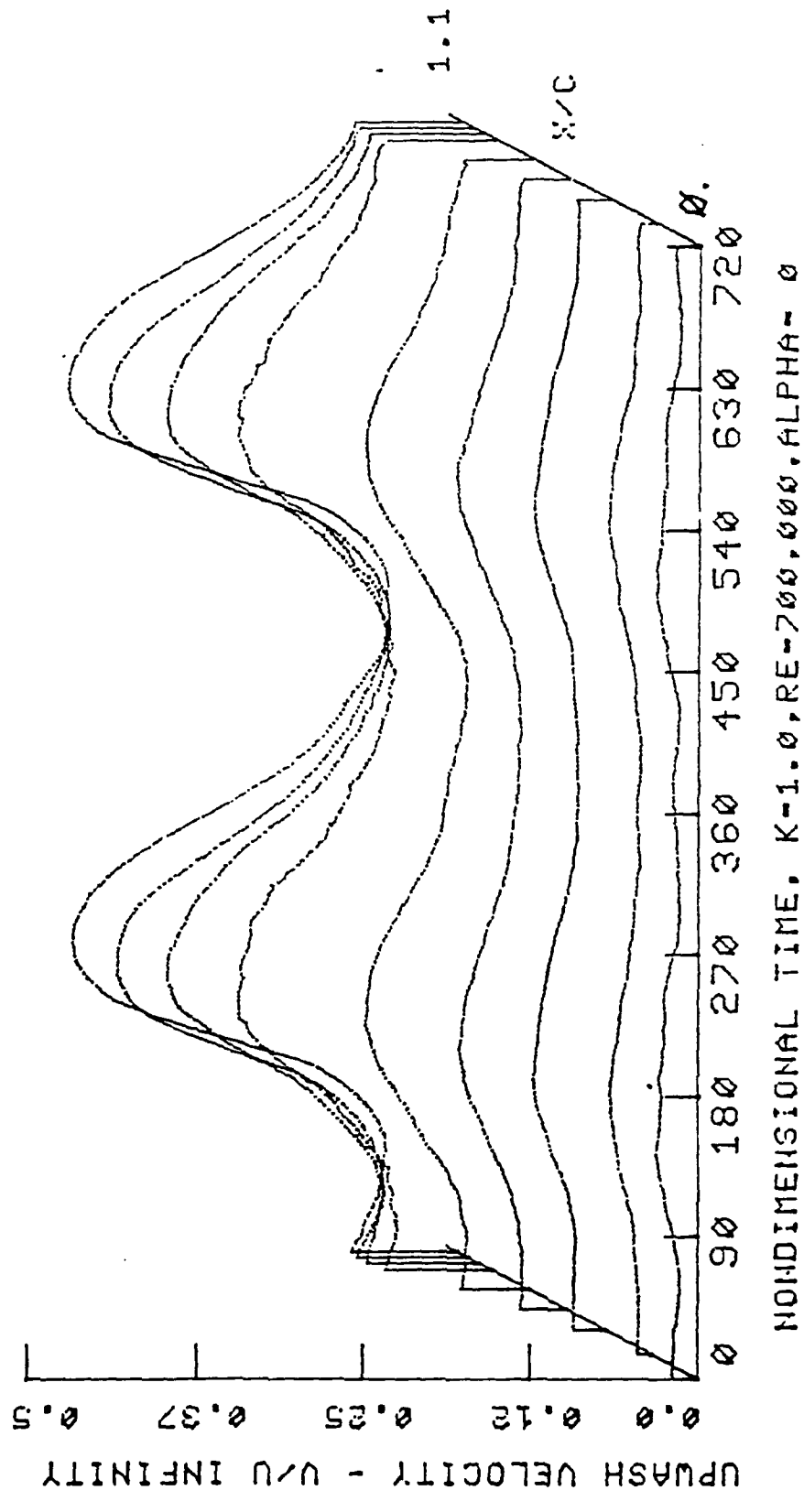
UPWASH VELOCITY - V/U INFINITY
0.0
0.12
0.25
0.37
0.5
0
90
180
270
360
450
540
630
720
NONDIMENSIONAL TIME, K-1.0,RE-700,000,ALPHA- 0
X/C
1.1
0.

FIGURE 4

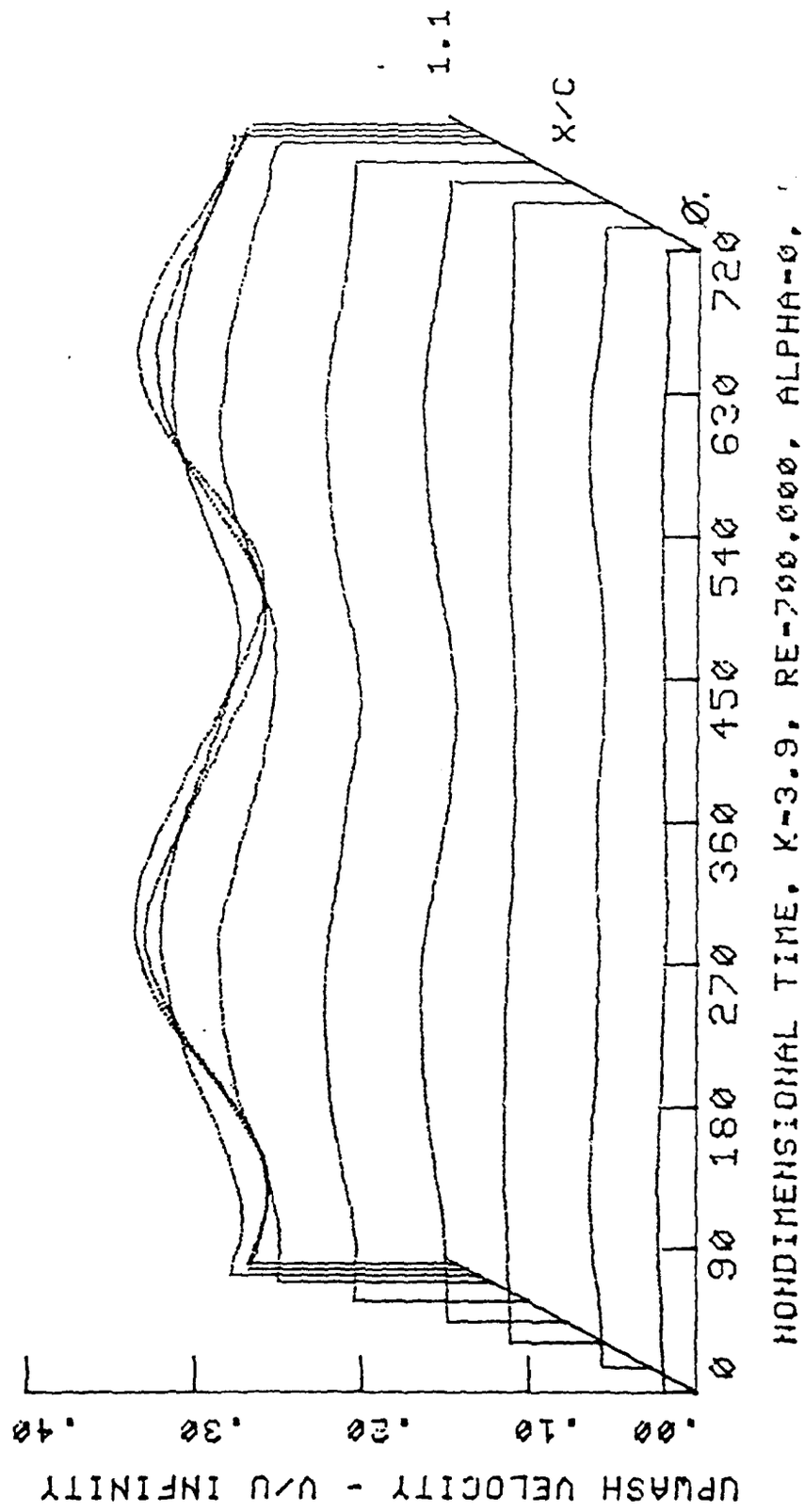
UPWASH VELOCITY - V/U INFINITY
.00
.10
.20
.30
.40
0
90
180
270
360
450
540
630
720
NONDIMENSIONAL TIME, K=3.9, RE=700,000, ALPHA=0,
X/C
1.1
0.

FIGURE 5

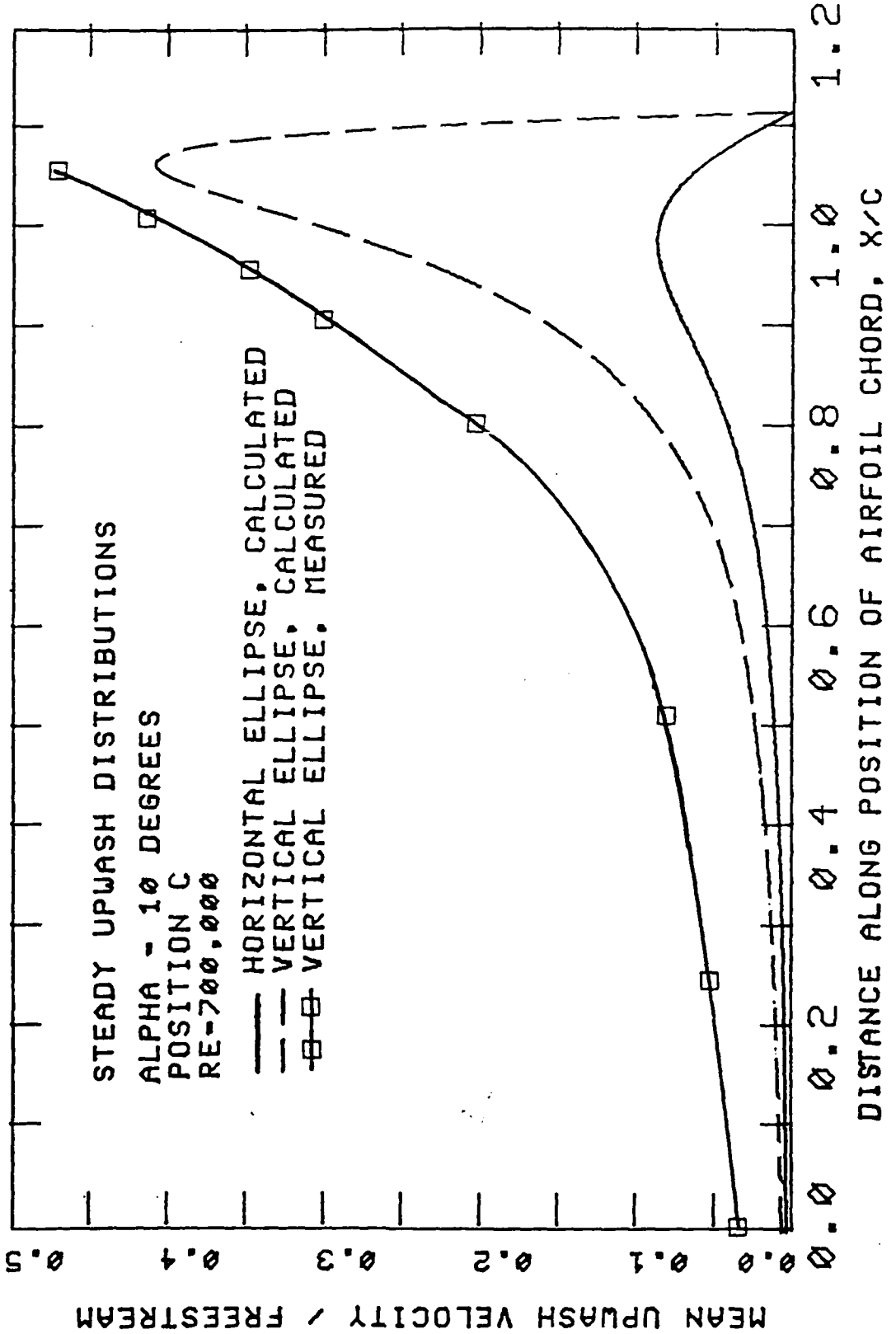
STEADY UPWASH DISTRIBUTIONS
ALPHA - 10 DEGREES
POSITION C
RE-700,000
HORIZONTAL ELLIPSE, CALCULATED
VERTICAL ELLIPSE, CALCULATED
VERTICAL ELLIPSE, MEASURED
MEAN UPWASH VELOCITY / FREESTREAM
0.0
0.1
0.2
0.3
0.4
0.5
0.0
0.2
0.4
0.6
0.8
1.0
1.2
DISTANCE ALONG POSITION OF AIRFOIL CHORD, X/C

FIGURE 6

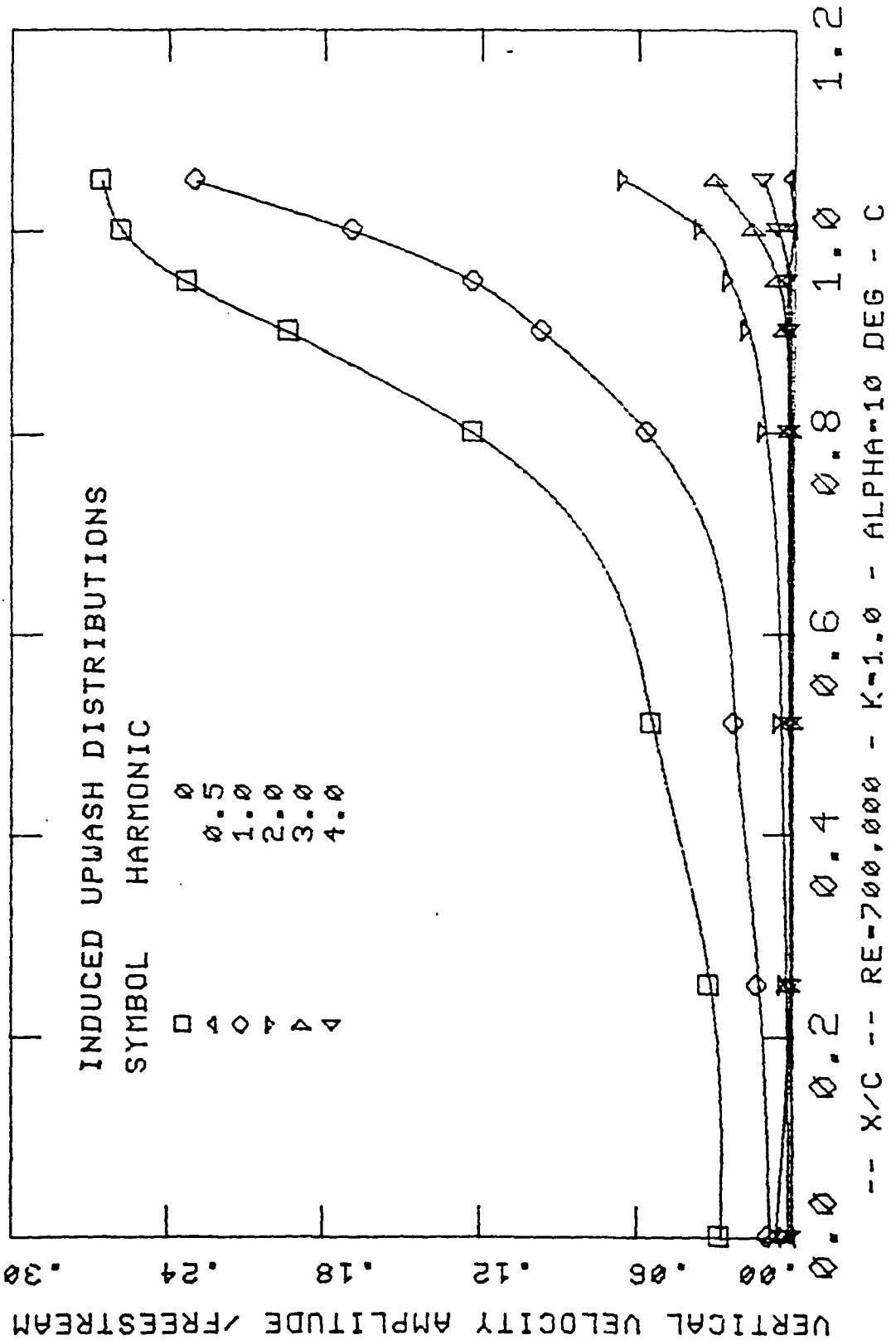
INDUCED UPWASH DISTRIBUTIONS
SYMBOL HARMONIC
0
0.5
1.0
2.0
3.0
4.0
VERTICAL VELOCITY AMPLITUDE /FREESTREAM
.00
.06
.12
.18
.24
.30
0.0
0.2
0.4
0.6
0.8
1.0
1.2
-- X/C -- RE=700,000 - K=1.0 - ALPHA=10 DEG - C

FIGURE 7

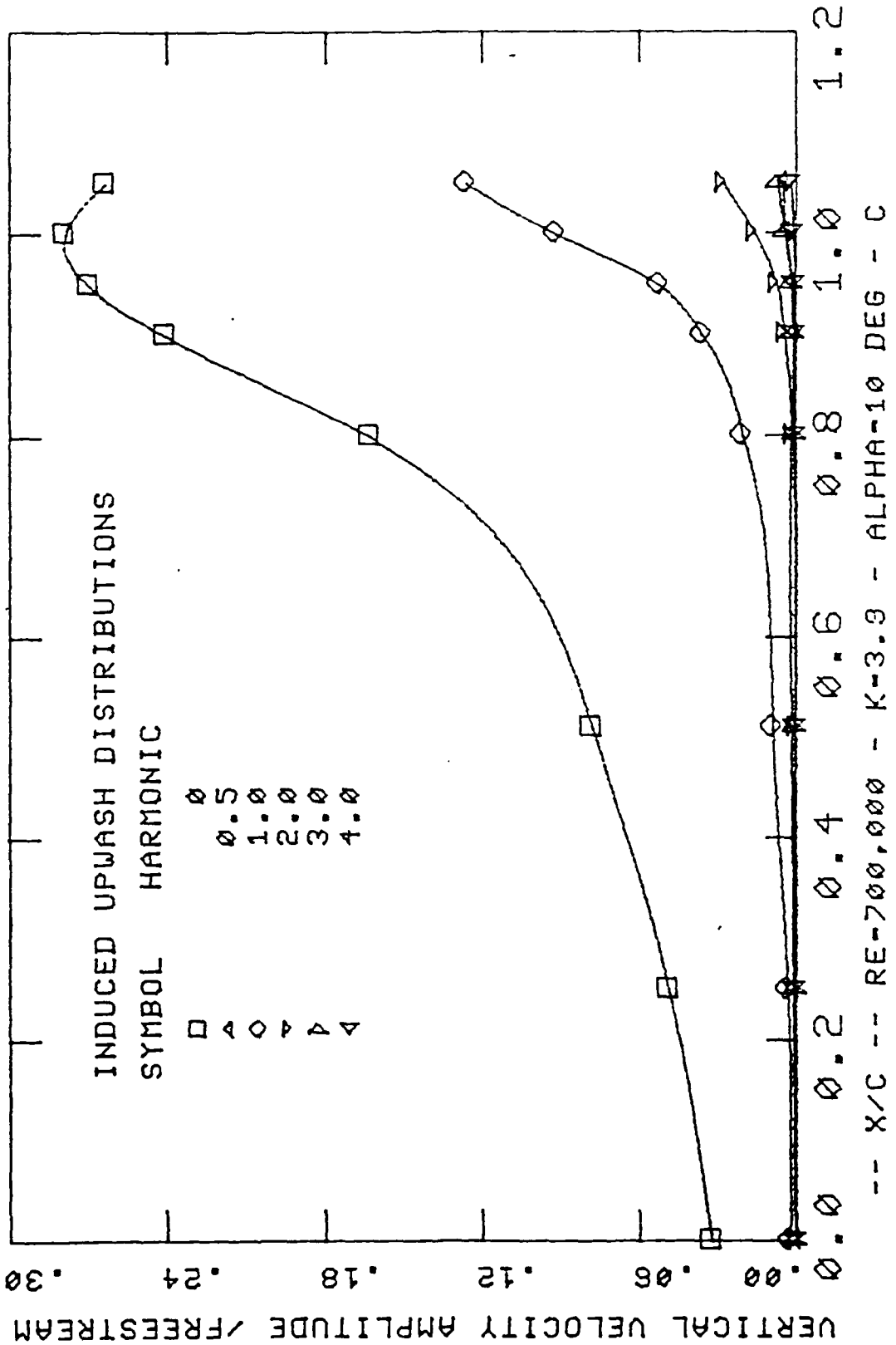
INDUCED UPWASH DISTRIBUTIONS
SYMBOL HARMONIC
0
0.5
1.0
2.0
3.0
4.0
VERTICAL VELOCITY AMPLITUDE /FREESTREAM
.00
.06
.12
.18
.24
.30
0.0
0.2
0.4
0.6
0.8
1.0
1.2
-- X/C -- RE-700,000 - K-3.3 - ALPHA-10 DEG - C

FIGURE 8

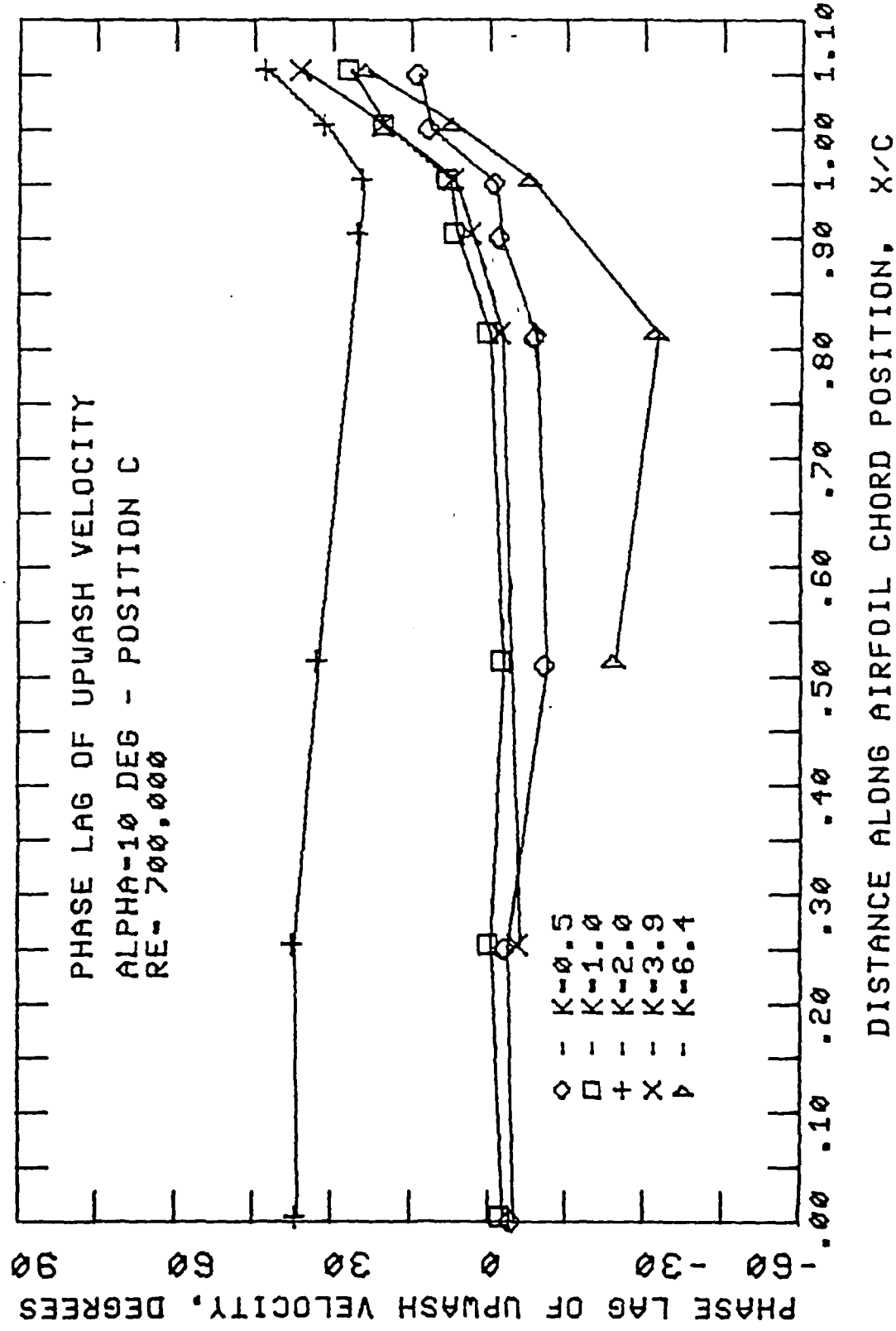
PHASE LAG OF UPWASH VELOCITY
ALPHA-10 DEG - POSITION C
RE- 700,000
K-0.5
K-1.0
K-2.0
K-3.9
K-6.4
PHASE LAG OF UPWASH VELOCITY, DEGREES
90
60
30
0
-30
-60
.00
.10
.20
.30
.40
.50
.60
.70
.80
.90
1.00
1.10
DISTANCE ALONG AIRFOIL CHORD POSITION, X/C

FIGURE 9

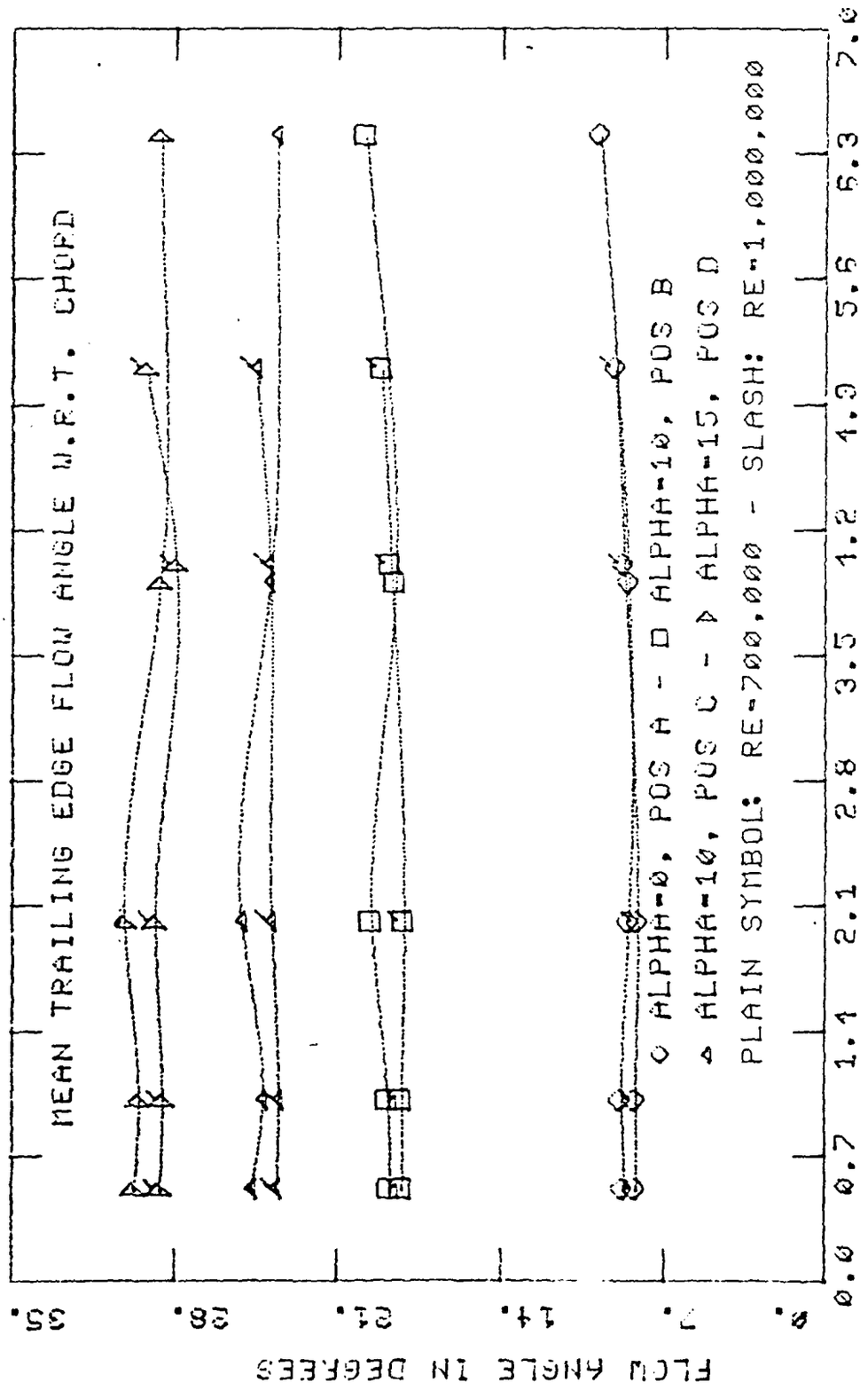
MEAN TRAILING EDGE FLOW ANGLE W.R.T. CHORD
◇ ALPHA=0, POS A - □ ALPHA=10, POS B
△ ALPHA=10, POS C - ▷ ALPHA=15, POS D
PLAIN SYMBOL: RE=700,000 - SLASH: RE=1,000,000
REDUCED FREQUENCY, K
0.0 0.7 1.1 2.1 2.8 3.5 1.2 1.9 5.5 5.3 7.0
FLOW ANGLE IN DEGREES
0. 7. 14. 21. 28. 35.

FIGURE 10

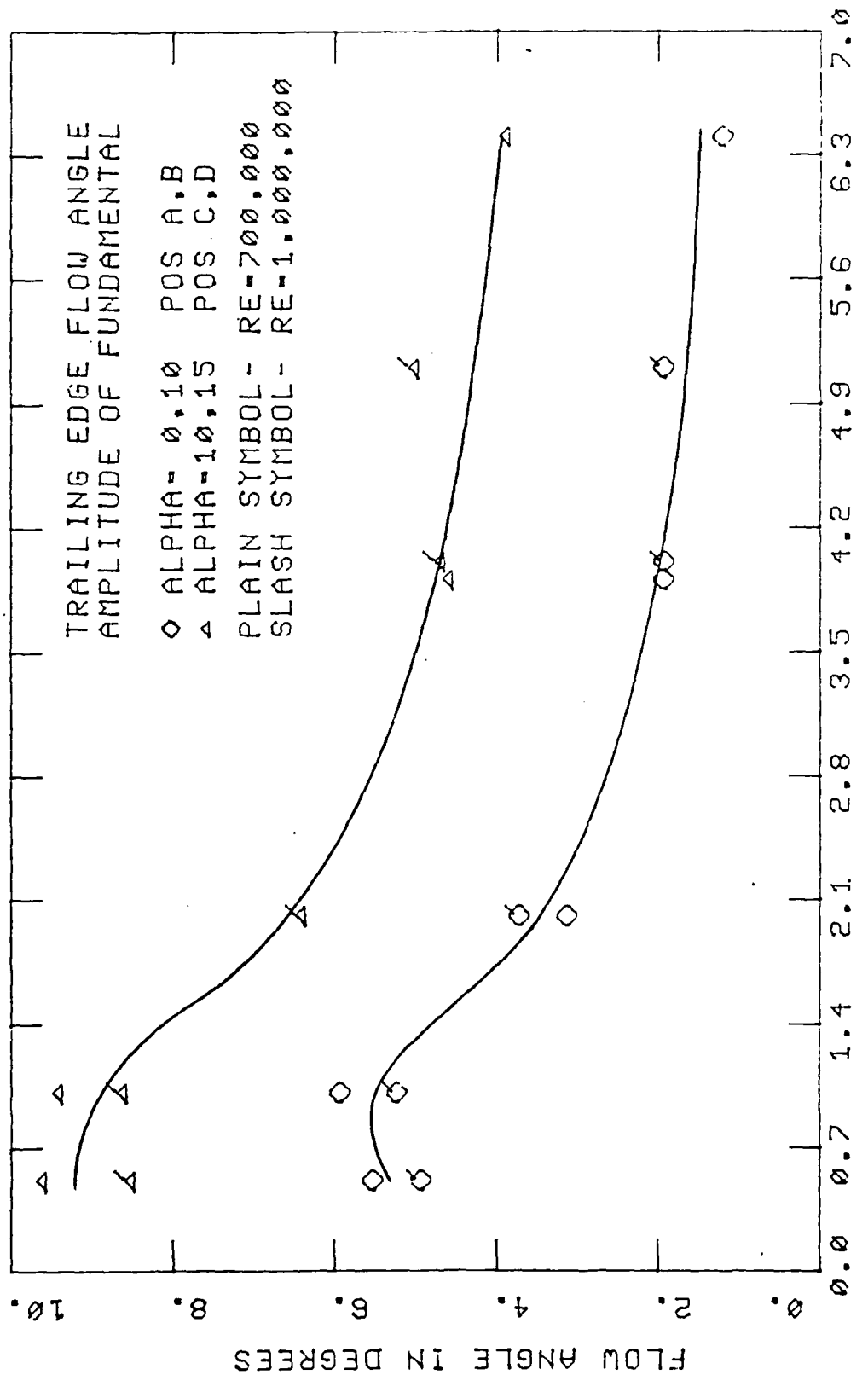
TRAILING EDGE FLOW ANGLE
AMPLITUDE OF FUNDAMENTAL
◇ ALPHA= 0.10 POS A,B
△ ALPHA=10.15 POS C,D
PLAIN SYMBOL- RE=700,000
SLASH SYMBOL- RE=1,000,000
FLOW ANGLE IN DEGREES
0. 2. 4. 6. 8. 10.
0.0 0.7 1.4 2.1 2.8 3.5 4.2 4.9 5.6 6.3 7.0
REDUCED FREQUENCY, K

FIGURE 11

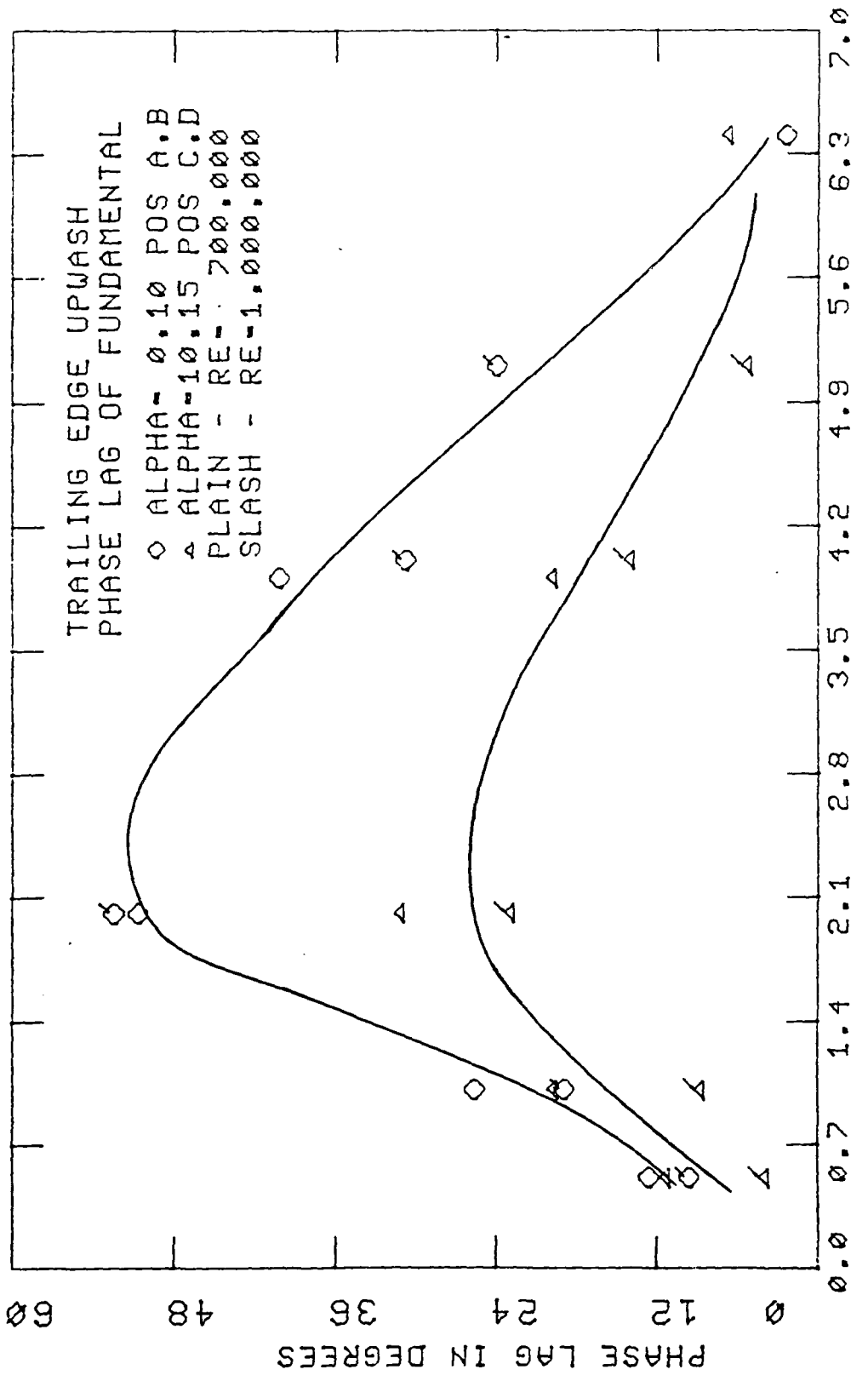
TRAILING EDGE UPWASH
PHASE LAG OF FUNDAMENTAL
◇ ALPHA= 0.10 POS A.B
△ ALPHA=10.15 POS C.D
PLAIN - RE= 700.000
SLASH - RE=1.000.000
PHASE LAG IN DEGREES
0
12
24
36
48
60
REDUCED FREQUENCY, K
0.0
0.7
1.4
2.1
2.8
3.5
4.2
4.9
5.6
6.3
7.0

FIGURE 12

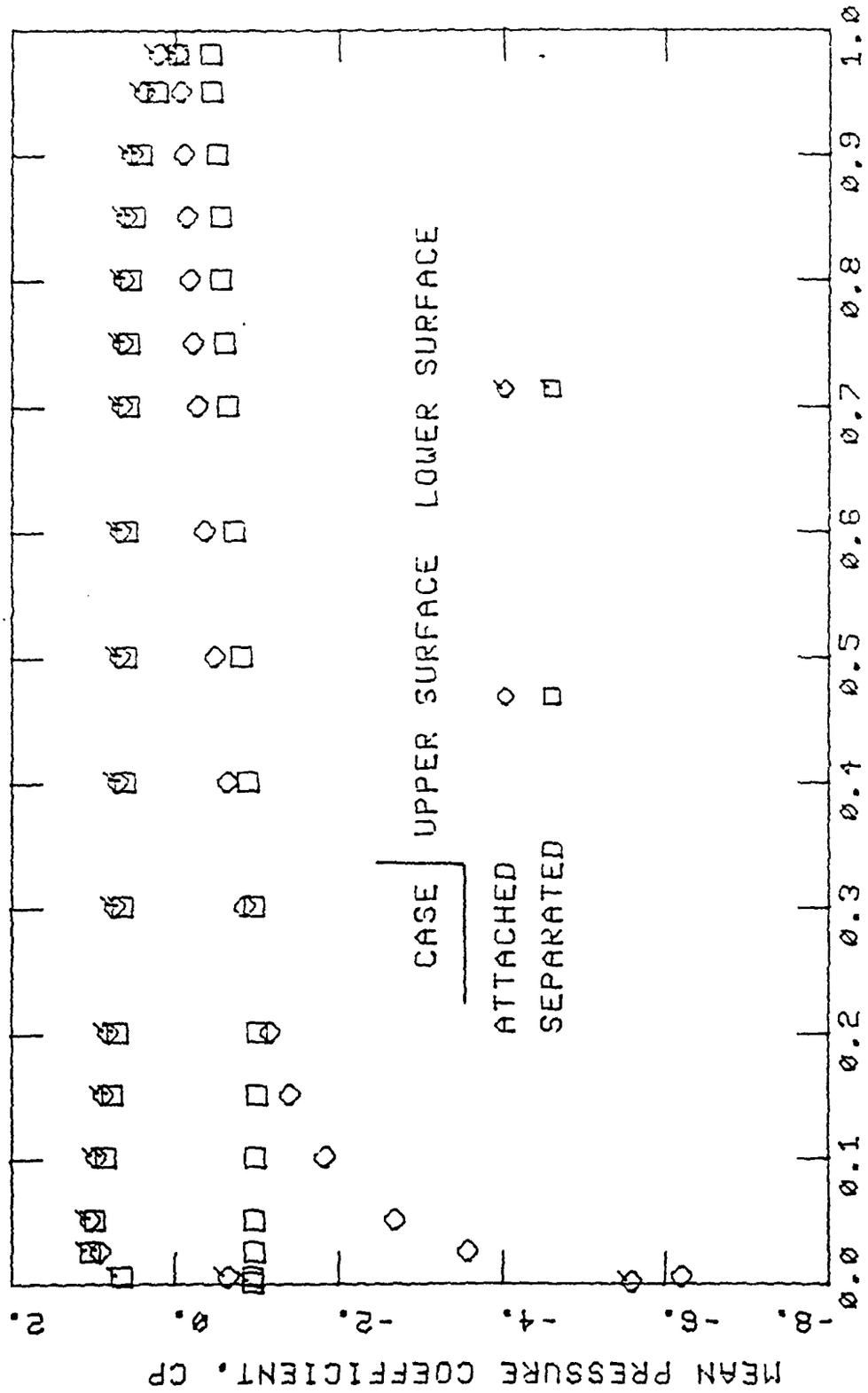
MEAN PRESSURE COEFFICIENT, CP
2.
0.
-2.
-4.
-6.
-8.
0.0
0.1
0.2
0.3
0.4
0.5
0.6
0.7
0.8
0.9
1.0
-- X/C -- K=6.1 - RE=700,000 - ALPHA=10 DEG - C -
CASE
ATTACHED
SEPARATED
UPPER SURFACE
LOWER SURFACE

FIGURE 13

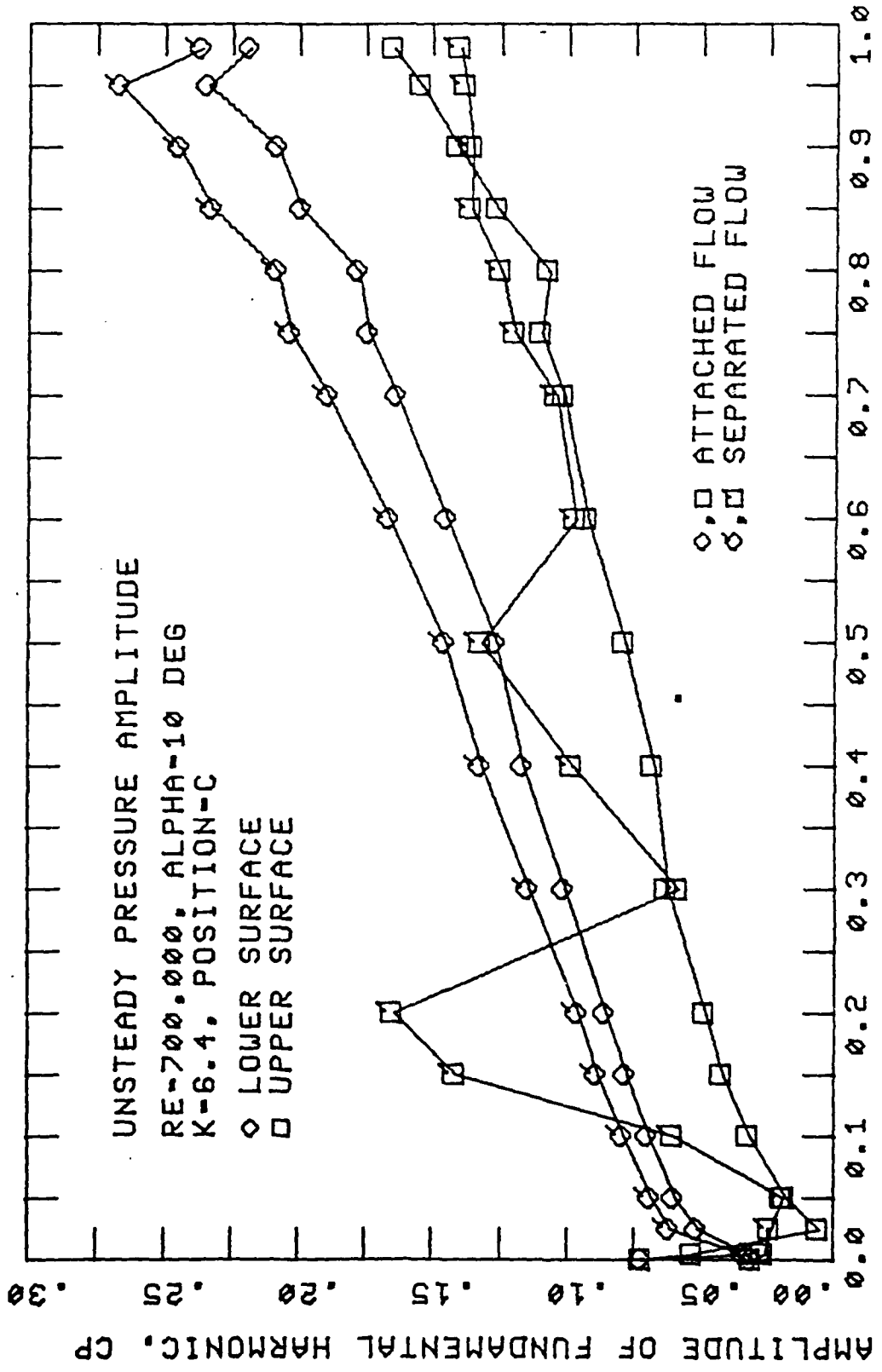
UNSTEADY PRESSURE AMPLITUDE
RE=700.000. ALPHA=10 DEG
K=6.4. POSITION=C
◇ LOWER SURFACE
□ UPPER SURFACE
◇,□ ATTACHED FLOW
◇,□ SEPARATED FLOW
AMPLITUDE OF FUNDAMENTAL HARMONIC, CP
.00
.05
.10
.15
.20
.25
.30
0.0
0.1
0.2
0.3
0.4
0.5
0.6
0.7
0.8
0.9
1.0
DISTANCE ALONG AIRFOIL CHORD, X/C

FIGURE 14

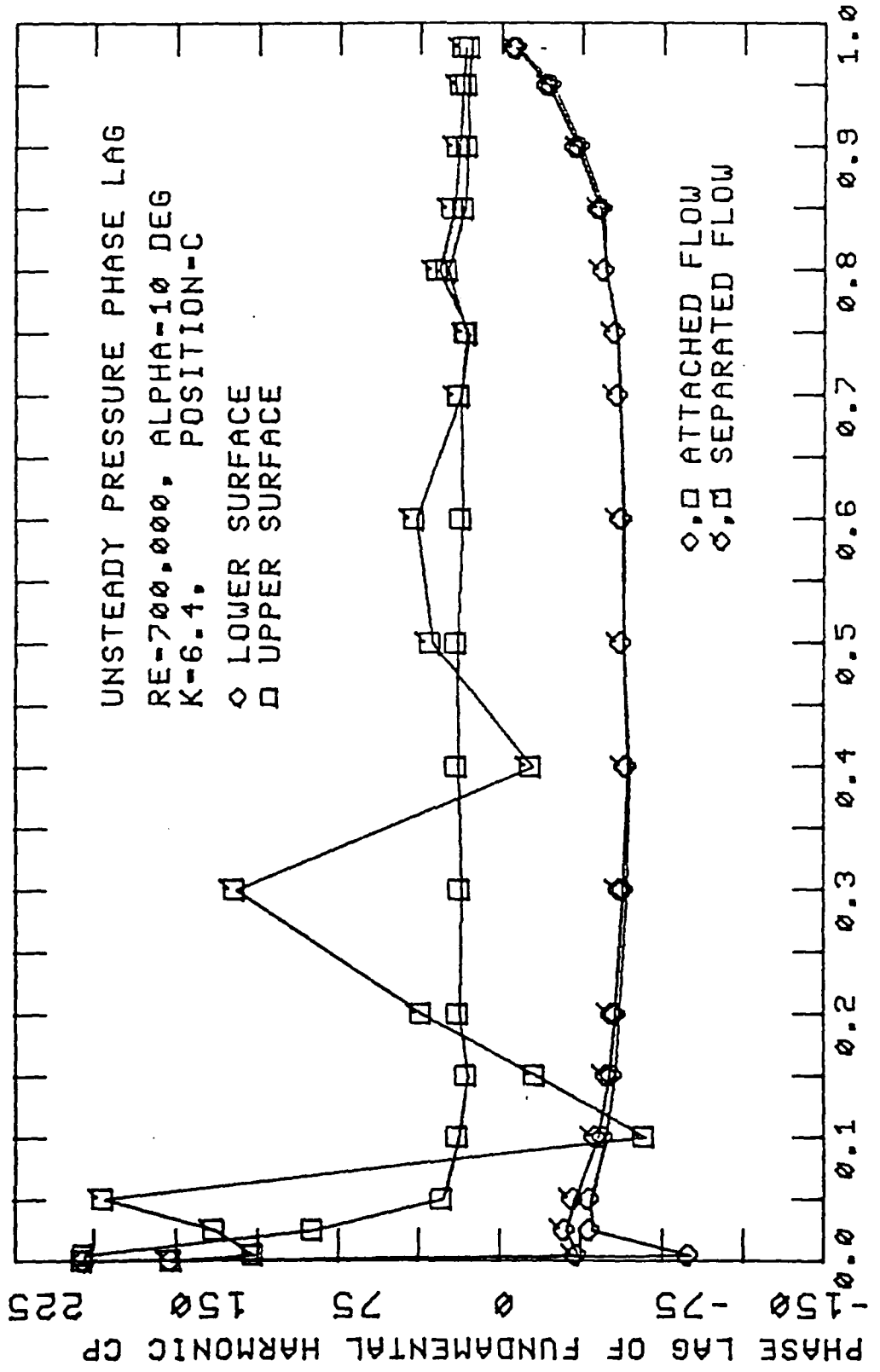
UNSTEADY PRESSURE PHASE LAG
RE=700,000, ALPHA=10 DEG
K=6.4, POSITION-C
◇ LOWER SURFACE
□ UPPER SURFACE
◇,□ ATTACHED FLOW
◇,□ SEPARATED FLOW
PHASE LAG OF FUNDAMENTAL HARMONIC CP
225
150
75
0
-75
-150
0.0
0.1
0.2
0.3
0.4
0.5
0.6
0.7
0.8
0.9
1.0
DISTANCE ALONG AIRFOIL CHORD, X/C

FIGURE 15

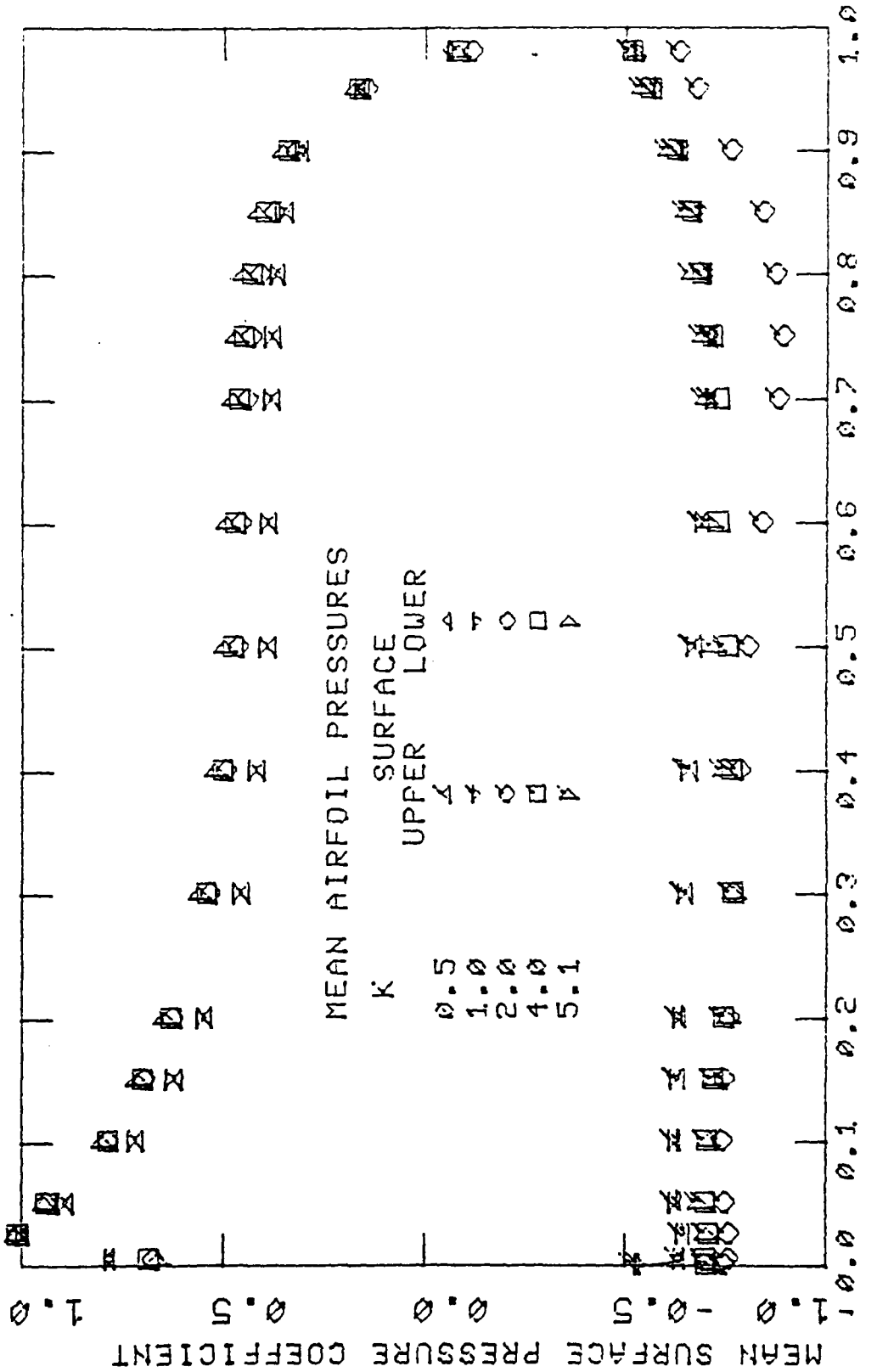
MEAN SURFACE PRESSURE COEFFICIENT
1.0
0.5
0.0
-0.5
-1.0
0.0
0.1
0.2
0.3
0.4
0.5
0.6
0.7
0.8
0.9
1.0
--- X/C ---
ALPHA = 1.5 DEG. RE = 1.000.000
MEAN AIRFOIL PRESSURES
SURFACE
UPPER
LOWER
K
0.5
1.0
2.0
4.0
5.1

FIGURE 16

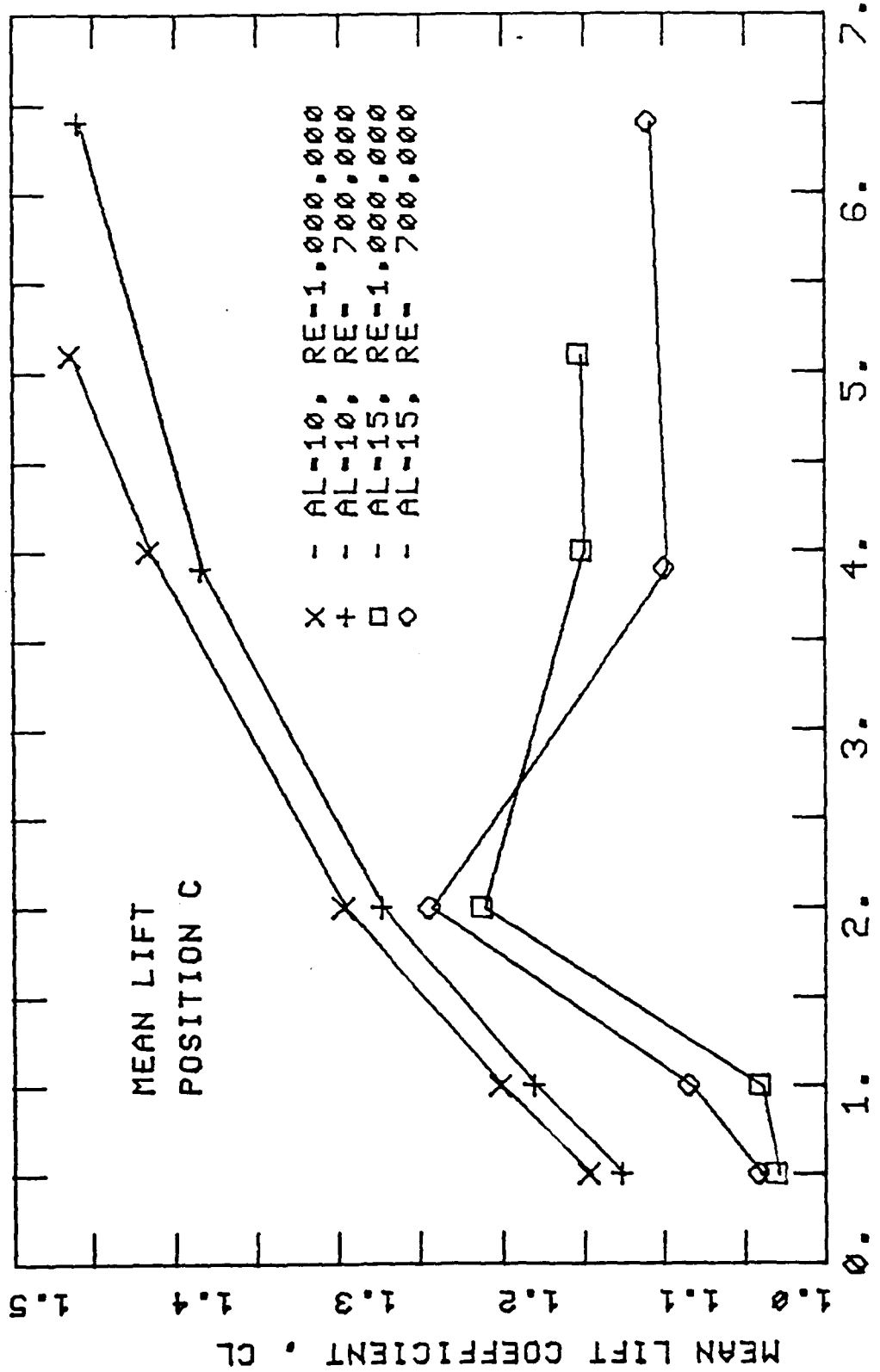
MEAN LIFT COEFFICIENT , CL
1.0
1.1
1.2
1.3
1.4
1.5
0.
1.
2.
3.
4.
5.
6.
7.
REDUCED FREQUENCY , K
MEAN LIFT
POSITION C
X - AL=10. RE=1,000,000
+ - AL=10. RE= 700,000
□ - AL=15. RE=1,000,000
◇ - AL=15. RE= 700,000

FIGURE 17

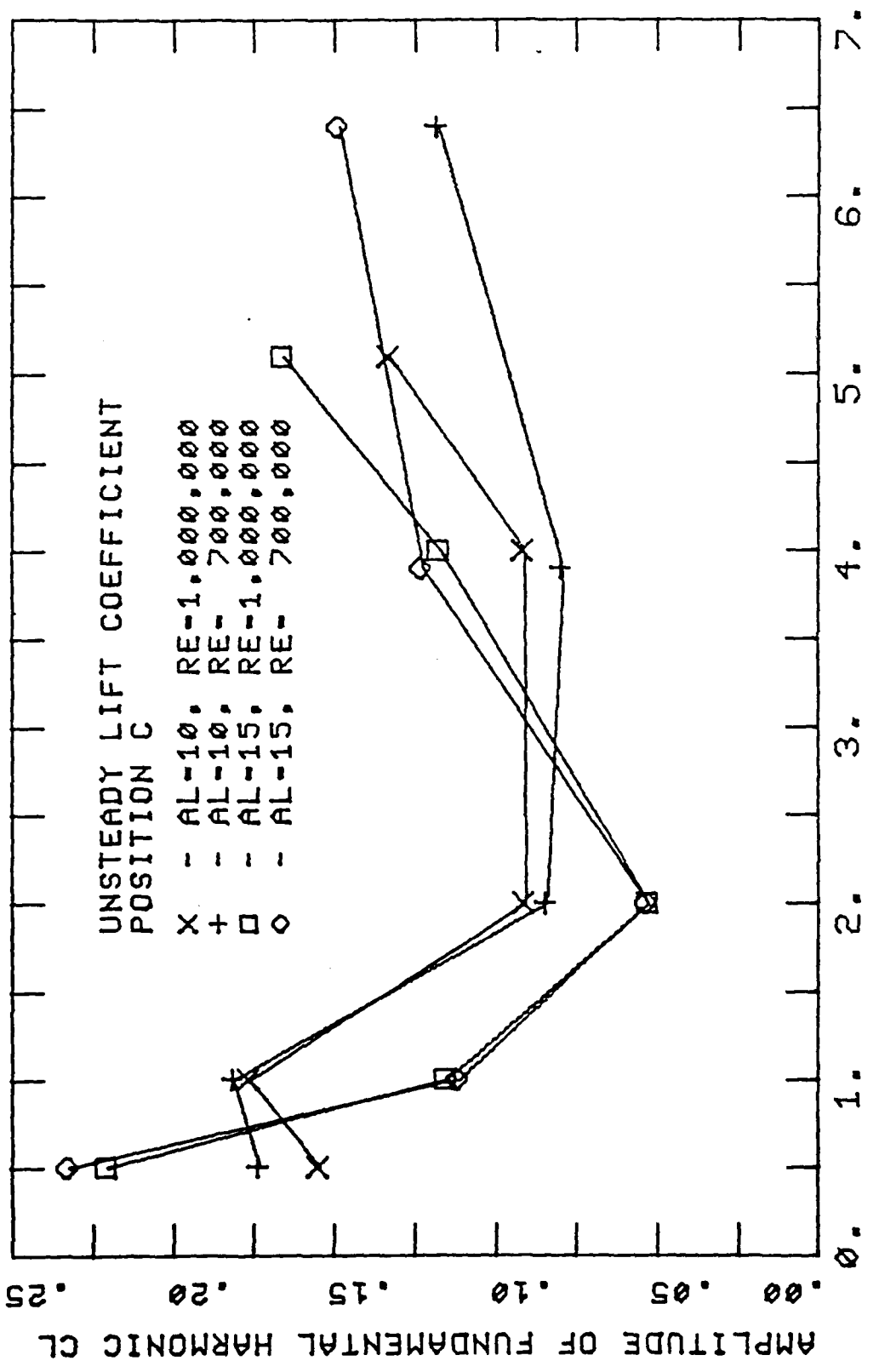
UNSTEADY LIFT COEFFICIENT
POSITION C
X - AL-10. RE-1.000.000
+ - AL-10. RE- 700.000
□ - AL-15. RE-1.000.000
◇ - AL-15. RE- 700.000
AMPLITUDE OF FUNDAMENTAL HARMONIC CL
.00
.05
.10
.15
.20
.25
0.
1.
2.
3.
4.
5.
6.
7.
REDUCED FREQUENCY, K

FIGURE 18

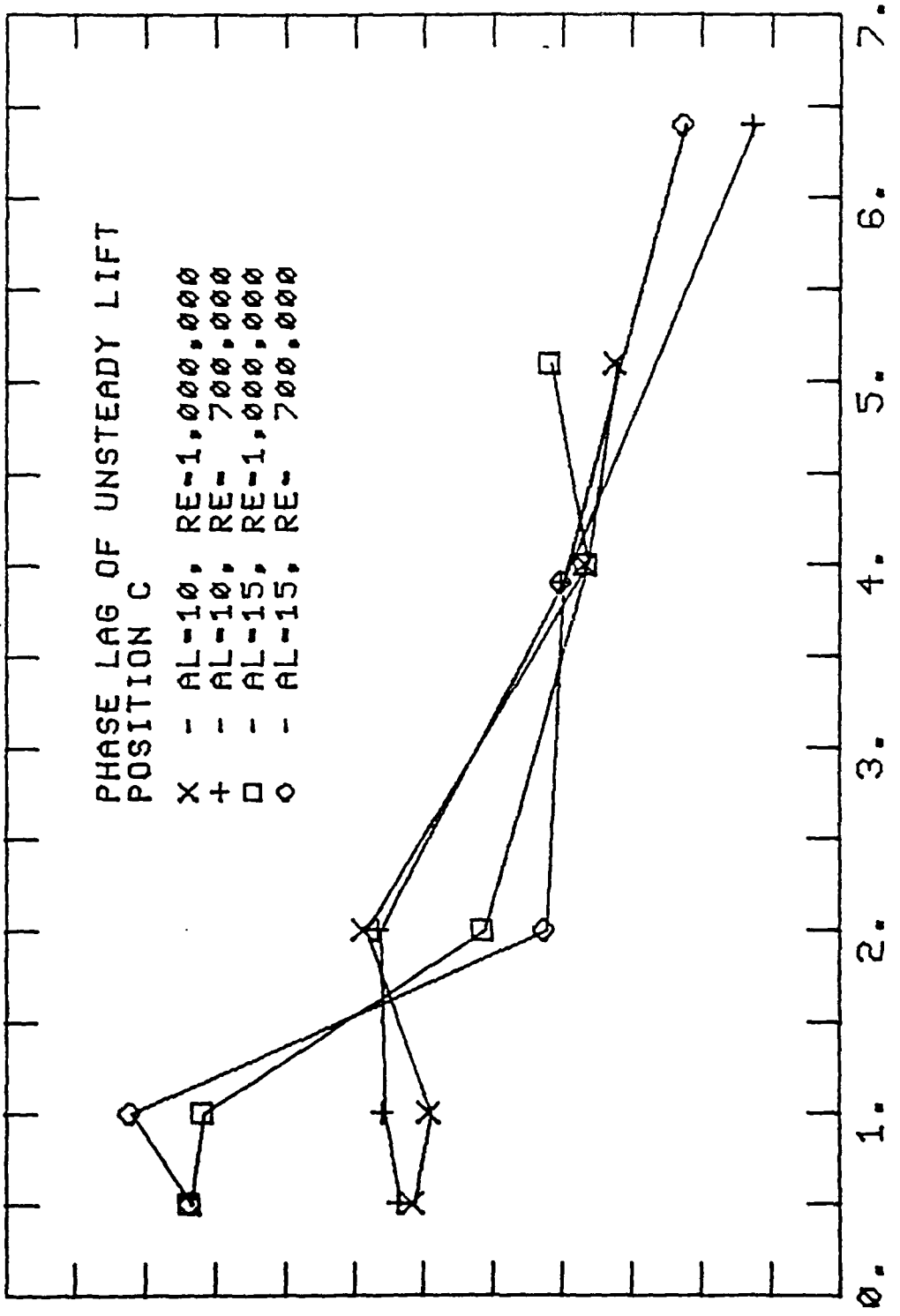
PHASE LAG OF UNSTEADY LIFT
POSITION C
X - AL-10, RE-1,000,000
+ - AL-10, RE- 700,000
□ - AL-15, RE-1,000,000
◇ - AL-15, RE- 700,000
PHASE LAG OF FUNDAMENTAL HARMONIC, DEG.
50
25
0
-25
-50
-75
-100
REDUCED FREQUENCY, K
0.
1.
2.
3.
4.
5.
6.
7.

FIGURE 19

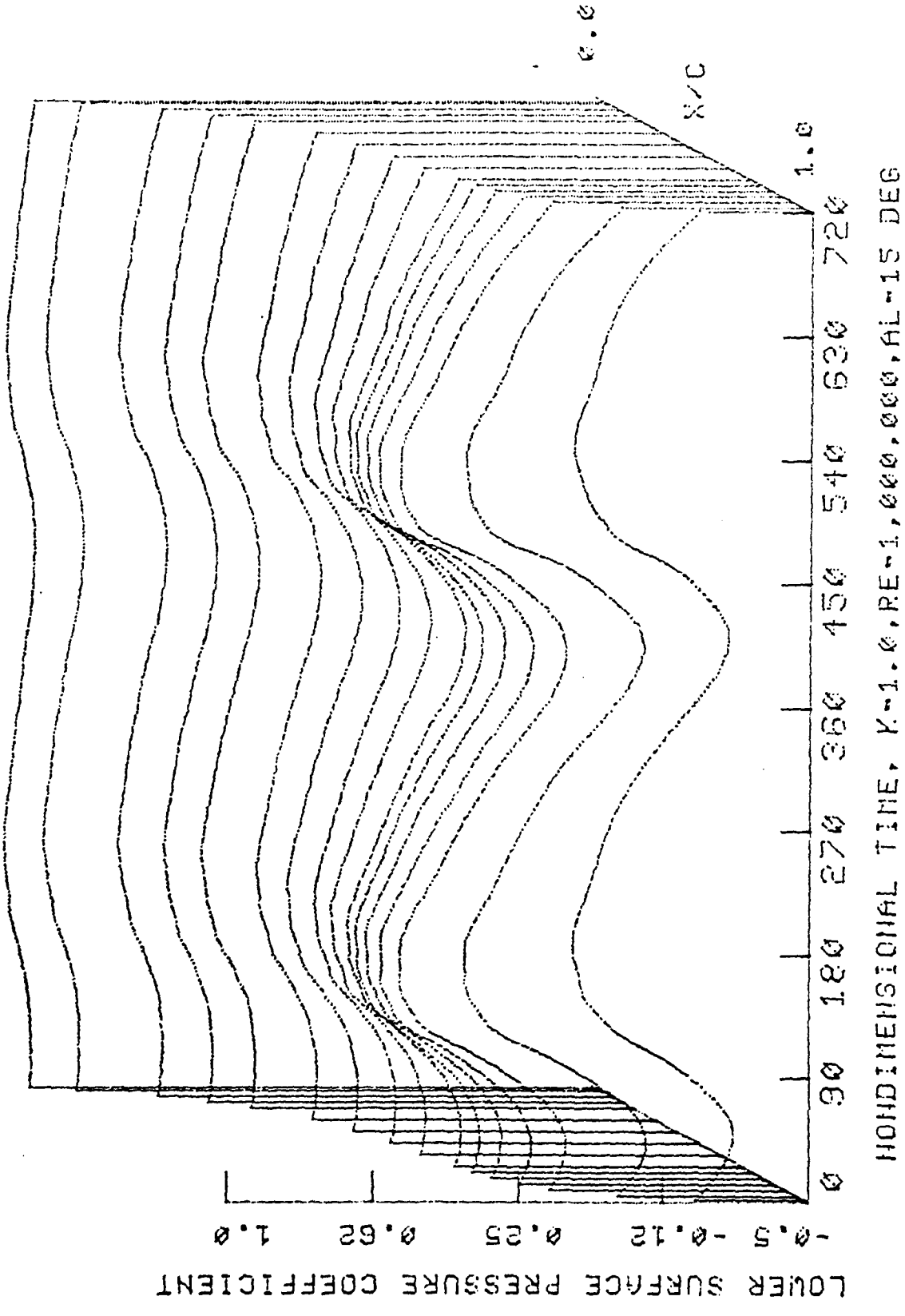
LOWER SURFACE PRESSURE COEFFICIENT
-0.5
-0.12
0.25
0.62
1.0
0
30
180
270
360
450
540
630
720
NONDIMENSIONAL TIME, M=1.6,RE=1,000,000,AL=15 DEG
X/C
0.0
1.0

FIGURE 20

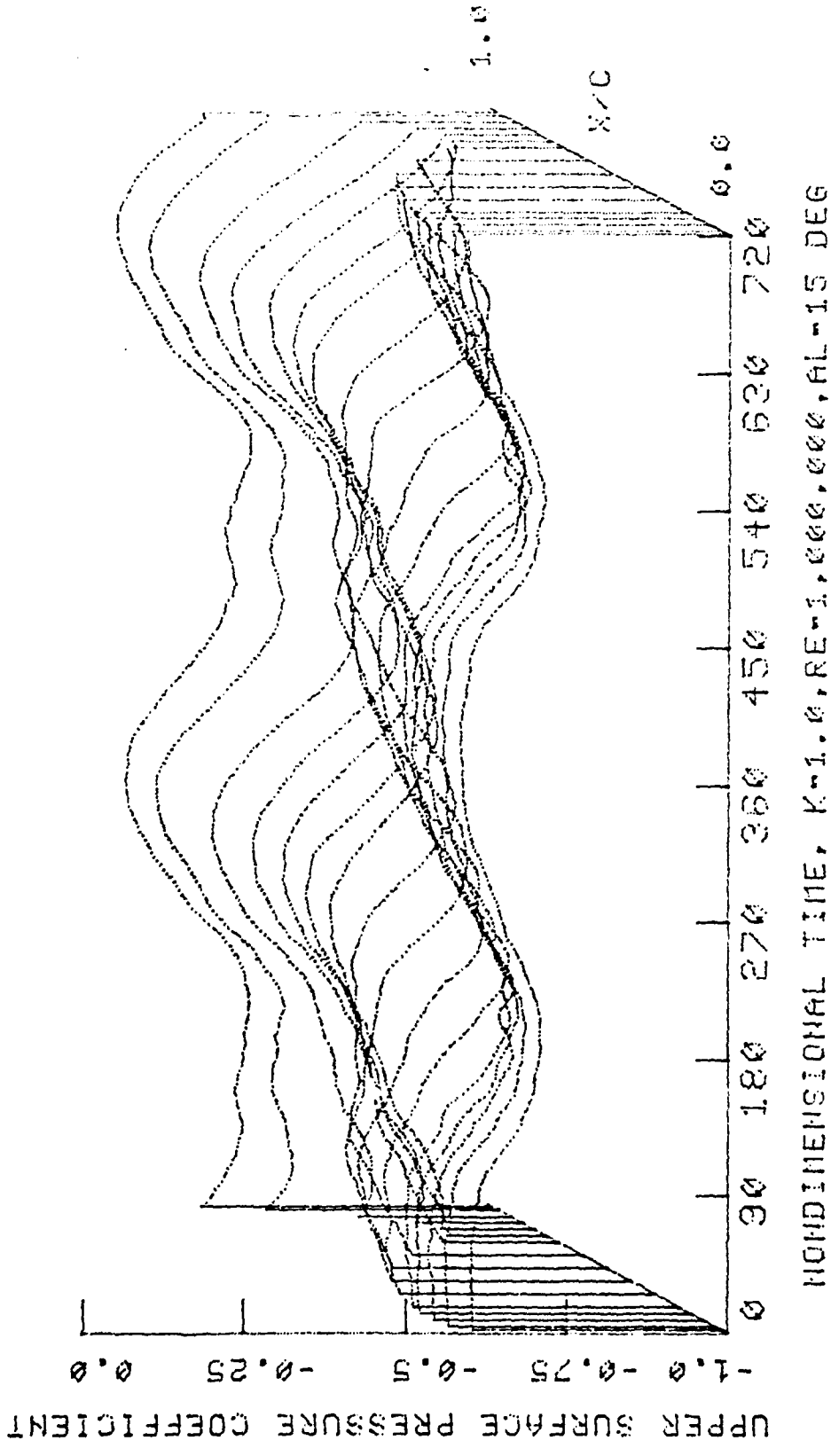
UPPER SURFACE PRESSURE COEFFICIENT
-1.0
-0.75
-0.5
-0.25
0.0
0
90
180
270
360
450
540
630
720
NONDIMENSIONAL TIME, K=1.0,RE=1,000,000,AL=15 DEG
X/C
0.0
1.0

FIGURE 21

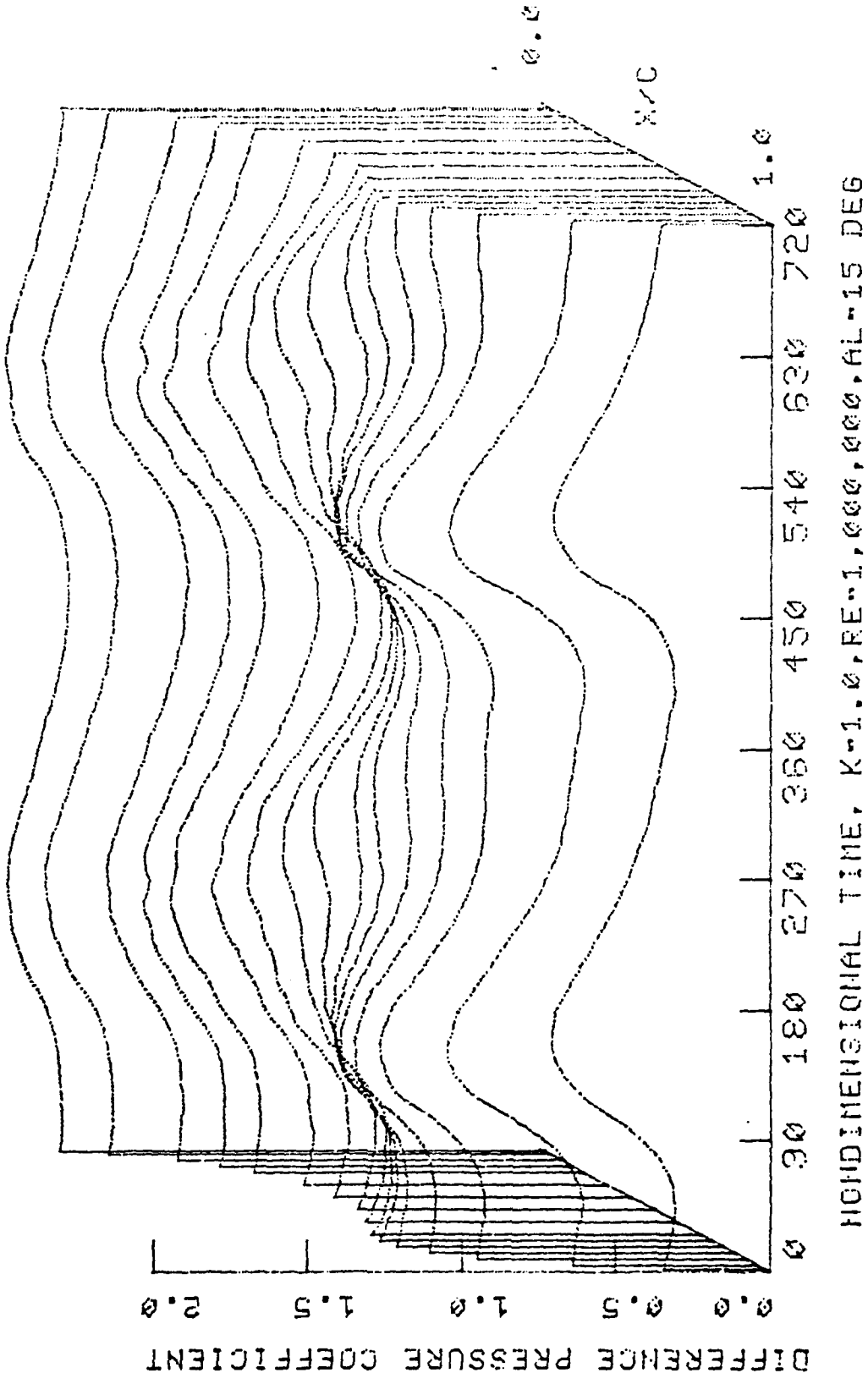
DIFFERENCE PRESSURE COEFFICIENT
0.0
0.5
1.0
1.5
2.0
0
90
180
270
360
450
540
630
720
NONDIMENSIONAL TIME, K=1.0,RE=1,000,000,AL=15 DEG
X/C
0.0
1.0

FIGURE 22

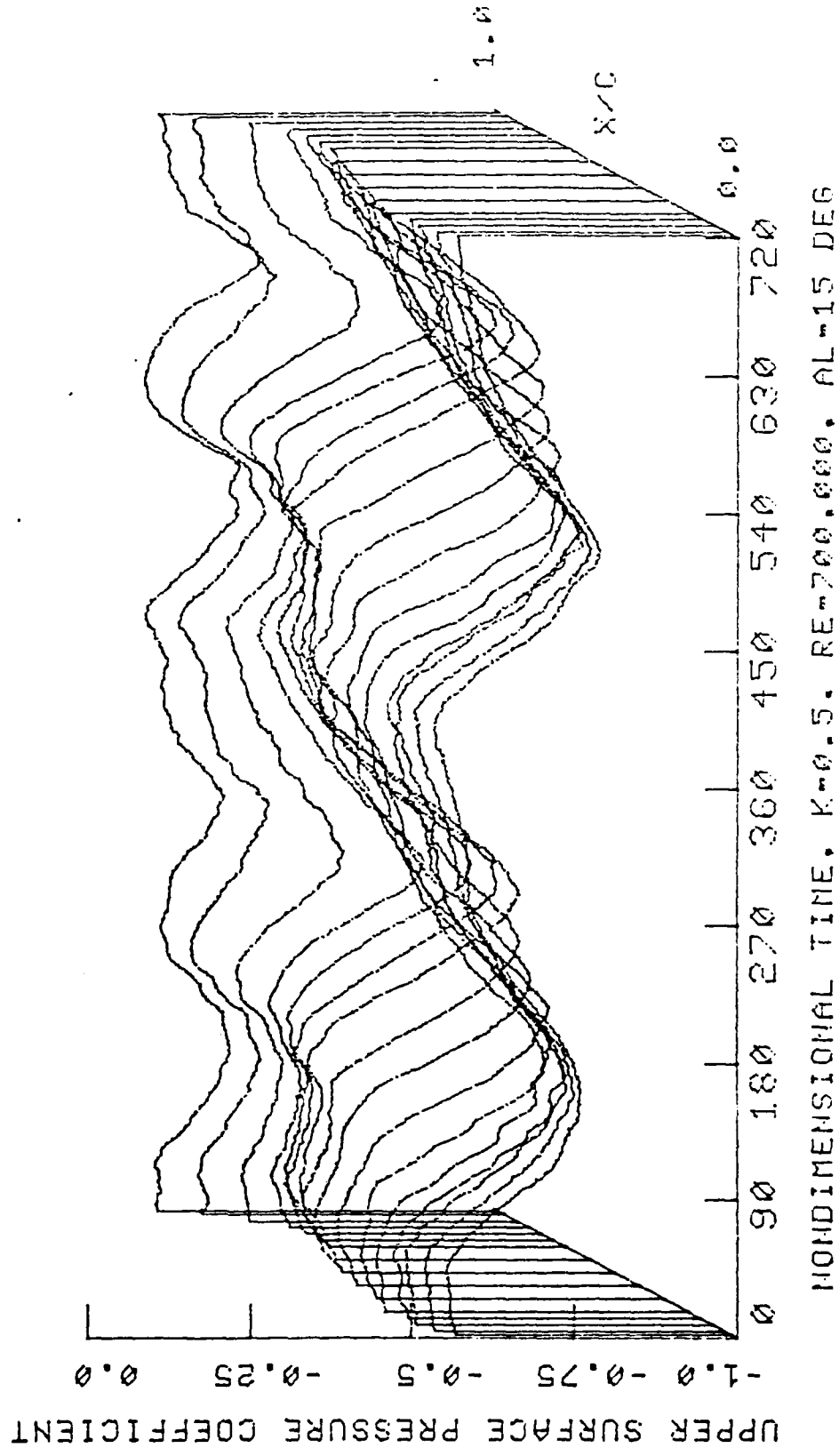
UPPER SURFACE PRESSURE COEFFICIENT
-1.0
-0.75
-0.5
-0.25
0.0
0
90
180
270
360
450
540
630
720
NONDIMENSIONAL TIME, K=0.5, RE=700,000, AL=15 DEG
X/C
1.0
0.0

FIGURE 23

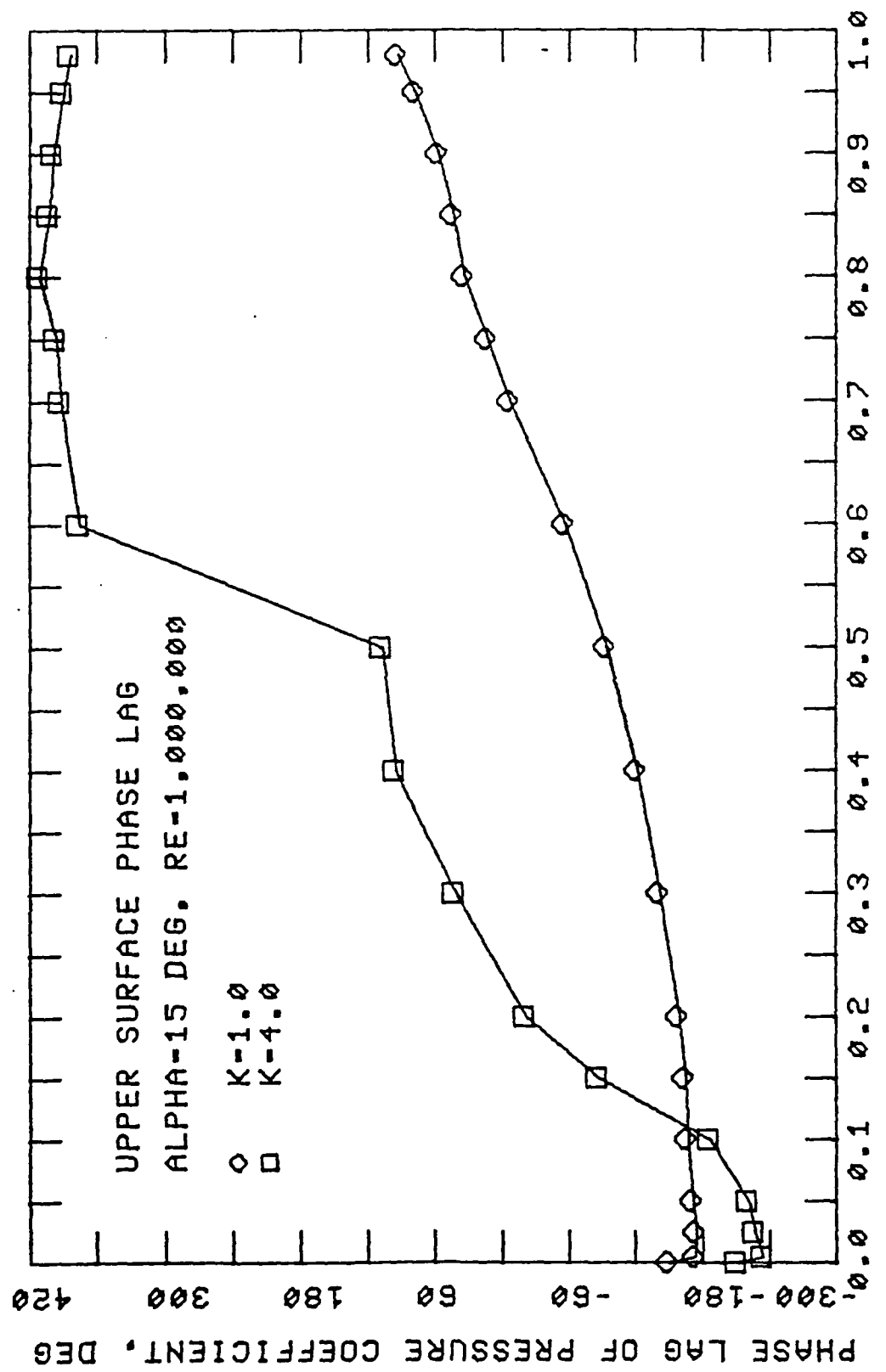
UPPER SURFACE PHASE LAG
ALPHA-15 DEG. RE-1,000,000
K-1.0
K-4.0
PHASE LAG OF PRESSURE COEFFICIENT, DEG
-300
-180
-60
60
180
300
420
0.0
0.1
0.2
0.3
0.4
0.5
0.6
0.7
0.8
0.9
1.0
DISTANCE ALONG AIRFOIL CHORD, X/C

FIGURE 24

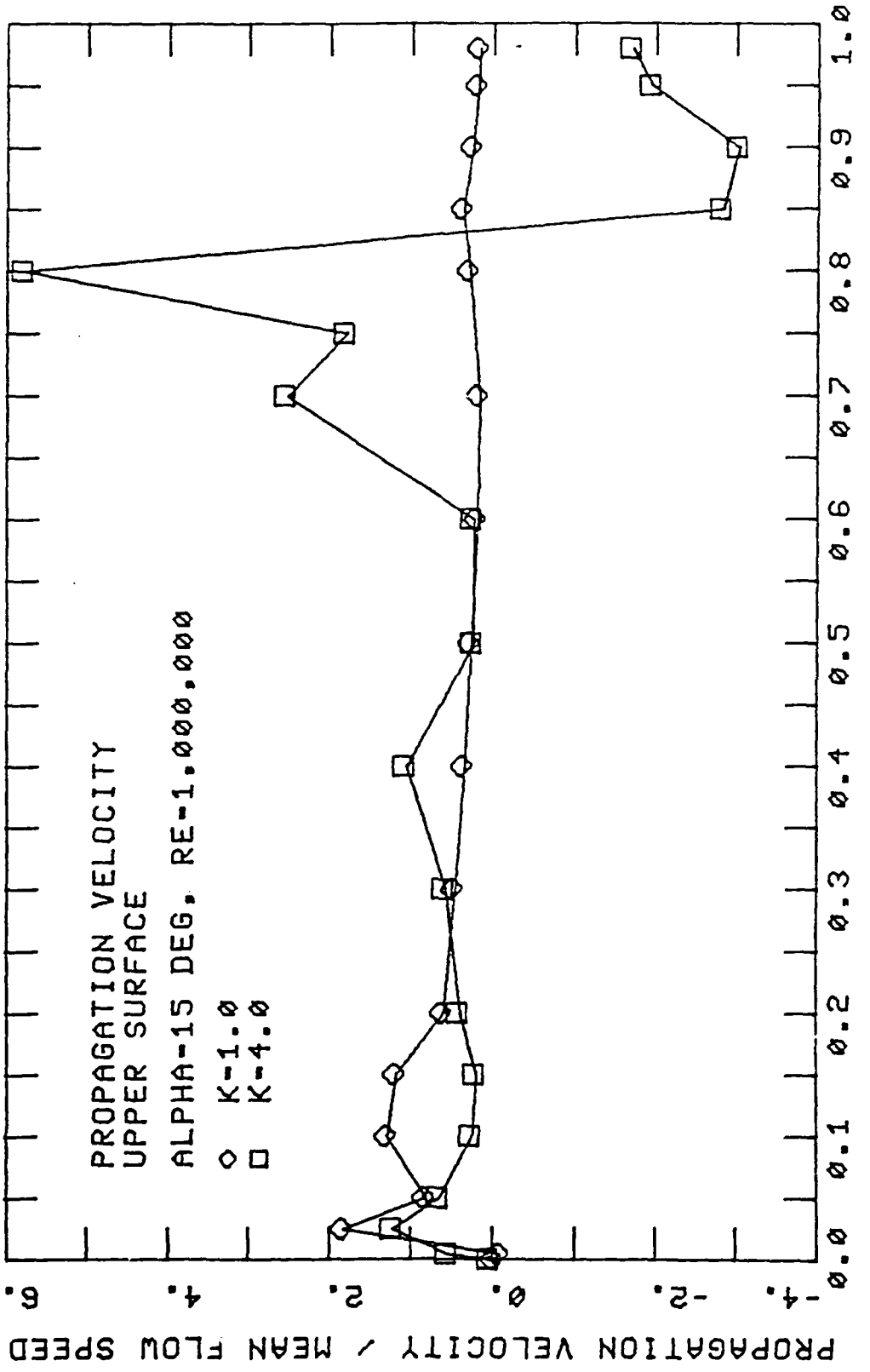
PROPAGATION VELOCITY
UPPER SURFACE
ALPHA-15 DEG. RE-1,000,000
◇ K-1.0
□ K-4.0
PROPAGATION VELOCITY / MEAN FLOW SPEED
6.
4.
2.
0.
-2.
-4.
0.0
0.1
0.2
0.3
0.4
0.5
0.6
0.7
0.8
0.9
1.0
DISTANCE ALONG AIRFOIL CHORD, X/C

FIGURE 25